Supporting Information

Integrating Bifunctionality and Chemical Stability in Covalent Organic Frameworks via One-Pot Multicomponent Reactions for Solar-Driven H_2O_2 Production

Prasenjit Das,[†] Gouri Chakraborty,[#] Jérôme Roeser,[†] Sarah Vogl,[†] Jabor Rabeah,[‡] Arne Thomas*[,†]

[†]*Department of Chemistry/Functional Materials, Technische Universität Berlin Hardenbergstraße 40, 10623 Berlin, Germany*

[#]*BAM Federal Institute for Materials Research and Testing, Richard-Willstätter-Str. 11, 12489 Berlin, Germany*

[‡]*Leibniz-Institut für Katalyse e.V. an der Universität Rostock, Albert-Einstein-Str. 29a, 18059 Rostock, Germany*

E-mail: *arne.thomas@tu-berlin.de*

Table of Contents

Section S1. General Methods and Materials

Materials. All purchased chemicals were used without further purification except where otherwise noted. *o*-DCB (1,2-Dichlorobenzene, 99%) anhydrous *n*-BuOH (*n*-Butanol, 99%), benzyl alcohol (BA), *t*-butyl alcohol (TBA), benzyl amine and styrene were purchased from Sigma Aldrich Chemicals. Tta (2,4,6-Tris(4-aminophenyl)triazine, 95%), Tpa-CHO (1,3,5-Tris(4-formylphenyl)triazine, >96.0%), Pyruvic acid were all supplied by TCI. Acetic acid (>99.0%), methanol (MeOH), Isopropanol (IPA), Ethanol (EtOH), were purchased from Carl Roth.

X-ray Powder Diffraction patterns was collected on a Bruker D8 Advance diffractometer in reflection geometry operating with a Cu Kα anode (λ = 1.54178 Å) operating at 40 kV and 40 mA. Samples were ground and mounted as loose powders onto a Si sample holder. PXRD patterns were collected from 2 to 60 2θ degrees with a step size of 0.02 degrees and an exposure time of 2 seconds per step.

^{1}H NMR Spectra for the samples dissolved in suitable solvents were carried on Bruker Avance II 400. ^{13}C Solid state NMR (cross polarization magic-angle spinning (CP/MAS)) spectra were carried out on a Bruker Avance 400 MHz spectrometer operating at 100.6 MHz.

Thermogravimetric Analyses (TGA) were performed using a TGA Q500 thermal analysis system under a N_2 atmosphere from room temperature to 800 °C at a ramping rate of 1 °C /min.

Attenuated Total Reflectance Fourier-Transform Infrared Spectrometry (ATR-FT-IR) was conducted using a PerkinElmer Spectrum Two spectrometer with diamond/ZnSe ATR accessory. All spectra were collected using a $LiTaO_3$ MIR detector over a range of 450 to 4000 cm^{-1}. All spectra were processed using Spectrum 10 software.

High Resolution-Mass Spectrometry (HR-MS) analyses were performed on a Shimadzu HRMS-2020 instrument using a 30-minute running time acetonitrile at a constant flow rate of 0.2 mL/min without passing through a column.

Solid-State Diffuse Reflectance Ultraviolet–Visible (UV-vis) Spectra of the pristine COF powders and starting monomers have been collected on Varian Cary 300 UV-vis Spectrophotometer.

X-ray Photoelectron Spectroscopy (XPS) was measured on a K-Alpha™ + X-ray Photoelectron Spectrometer System (Thermo Scientific) with Hemispheric 180 ° dual-focus analyzer with 128-channel detector. The X-ray monochromator used micro focused Al-Kα radiation. For the measurement, the powder samples were pressed and loaded on carbon tape, then pasted onto the sample holder for measurement. The data was collected with an X-ray spot size of 400 μm, 20 scans for the survey, and 50 scans for the regions.

Field Emission Scanning Electron Microscopy (**FESEM**) was measured on a ZEISS GeminiSEM500. All the COF materials were observed directly without gold coating in nanoVP mode.

High Resolution Transmission Electron Microscopy (HRTEM) was measured on a JEOL G-ARM STEM (JEM ARM300F2). All the COF samples were prepared on a carbon grid after suspension in a EtOH-acetonitrile mixture.

Nitrogen Sorption Measurements were performed at 77 K using an Autosorb-iQ-MP from Quantachrome. Prior to the analysis the samples were dried and degassed at 100 °C for 12 h.

HOMO-LUMO energy was calculated using DFT method with basis set B3LYP/6-31G+(d)).

Section S2. Synthesis and Characterization of Model Compound and COFs

Synthesis of Model Compound

A round-bottomed flask (25 mL) was charged with 3,4-dimethoxyaniline (100 mg, 0.17 mmol), salicaldehyde (60 mg, 0.17 mmol), pyruvic acid (PA) (0.6 mmol, 60 μL), 2,3-dichloro-5,6-dicyano-1,4-benzoquinone (DDQ) (5.4 mg, 0.02 mmol) in ethanol (5 mL). The reaction mixture was refluxed at 80 °C for 6 h. After finishing heating, the flask was cooled down and the reaction mixture was added dropwise to a beaker filled with ice. The formed precipitate was filtered and washed with water several times. Finally, the powder was dried in a normal oven at 60 °C. Yield = 82%. Suitable single crystals were grown from a mixture of solvents (acetone, methanol, ethanol and hexane (1:1:1:1)).

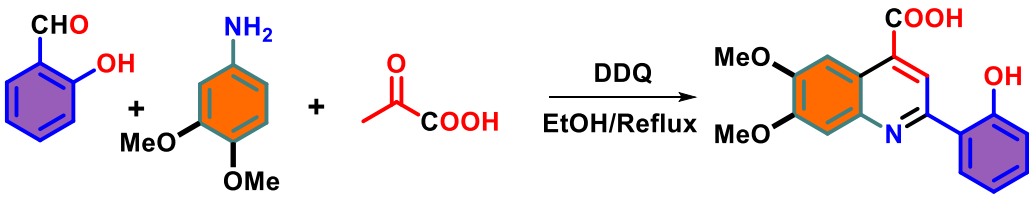

Scheme S1. Synthesis of the model compound**.**

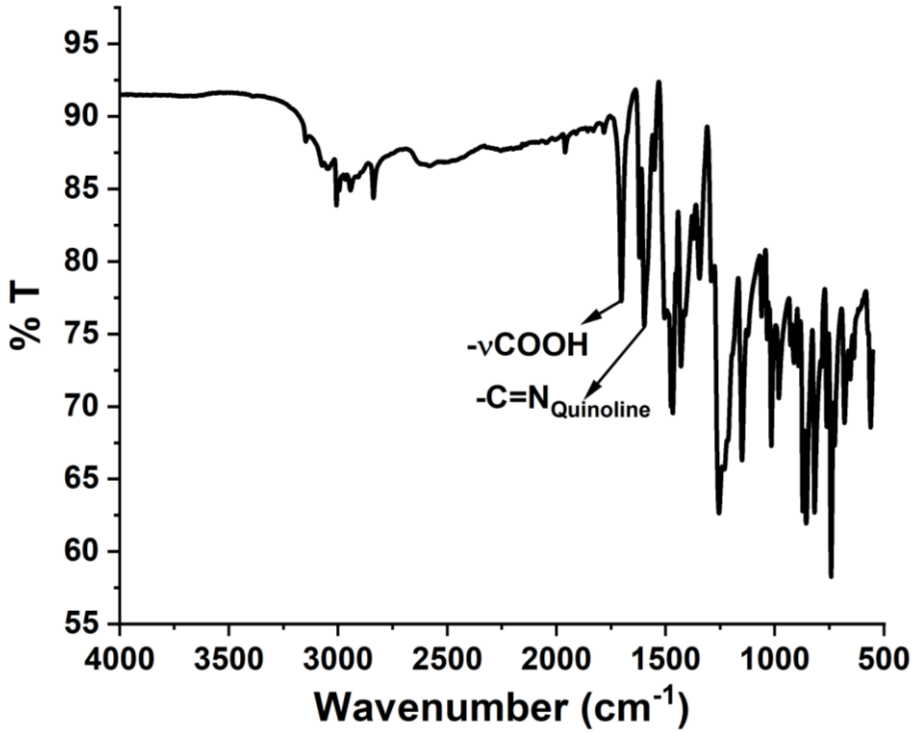

Figure S1. FTIR spectrum of the model compound.

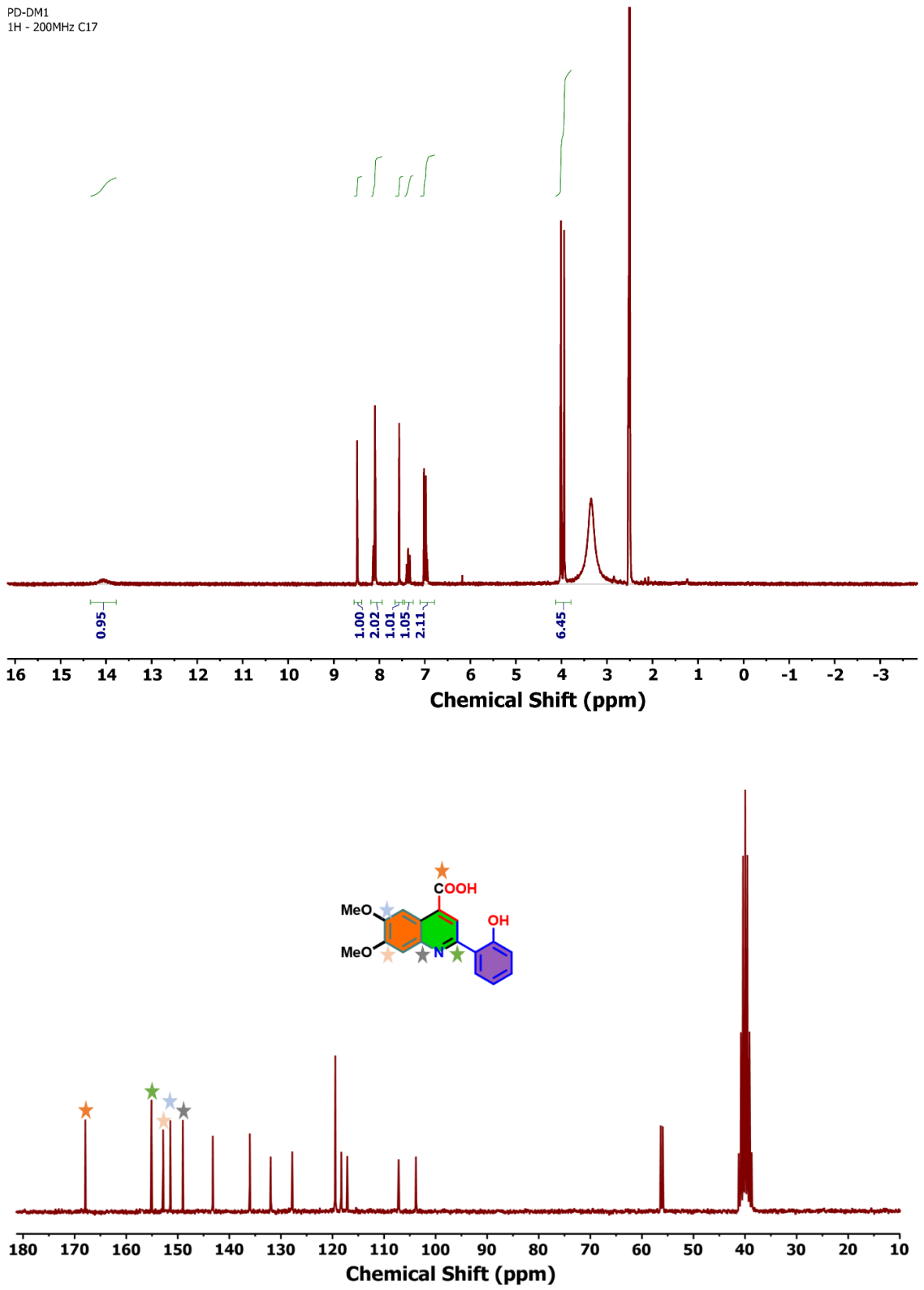

Figure S2. ^{1}H-NMR (top) and ^{13}C-NMR (bottom) spectra of the model compound.

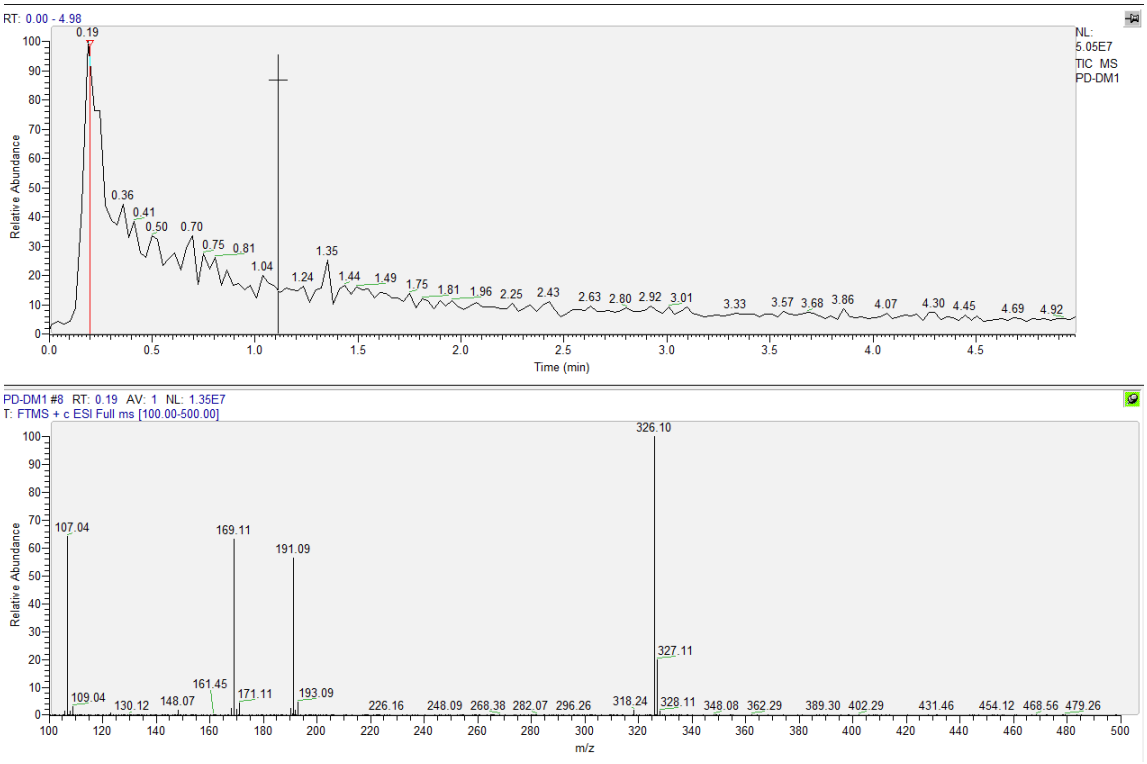

Figure S3. HRMS of model compound [M+H: 326.10].

Table S1. Crystallographic data and structure refinement parameters for the **Model compound**.

compound	**Model Compound**
CCDC No.	2208147
chemical formula	$C_{12}H_{10}N_{0.667}O_{3.333}$
formula weight (g mol^{-1})	216.882
temperature (K)	150.00(10)
wavelength (Å)	0.71073
crystal system	monoclinic
space group	$P2_1/n$
a (Å)	5.28232(13)
b (Å)	25.5797(6)
c (Å)	11.0770(3)
α (°)	90
β (°)	101.909(2)
γ (°)	90
Z	6
V (Å^3)	1464.52(6)
density (g/cm^3)	1.475
μ (mm^{-1})	0.712
F(000)	682.562
2θ (°) range for data collection	4.4020 to 72.539
no. of reflections collected	2864
no. of independent reflections	2490
no. of reflections with $I > 2\sigma(I)$	7746
R_{int}	0.1092
no. of parameters refined	212
GOF on F^2	1.0432
final $R_1{}^a$ / w$R_2{}^b$ (I >2σ(I))	0.0762/0.2177
$R_1{}^a$ / w$R_2{}^b$ (all data)	0.1479/0.3465
largest diff. peak and hole (e Å^{-3})	2.30/-1.06

$^a R_1 = \Sigma||F_o| - |F_c||/\Sigma|F_o|$. $^b wR_2 = [\Sigma w(F_o^2 - F_c^2)^2/\Sigma w(F_o^2)^2]^{1/2}$, where $w = 1/[\sigma^2(F_o^2) + (aP)^2 + bP]$, $P = (F_o^2 + 2F_c^2)/3$.

Synthesis of DMCR-1

A Pyrex glass tube (15 mL) was charged with 2,4,6-Tris(4-aminophenyl)triazine (56 mg, 0.17 mmol), 4,4',4''-(1,3,5-triazine-2,4,6-triyl)tribenzaldehyde (60 mg, 0.17 mmol), pyruvic acid (PA) (0.6 mmol, 60 μL), 2,3-dichloro-5,6-dicyano-1,4-benzoquinone (DDQ) (10 mg, 0.04 mmol), 1.5 mL *o*-DCB and 1.5 mL *n*-BuOH. The tube was first sonicated for 20 minutes and then flash frozen at 77 K (liquid N_2 bath) and degassed by three freeze-pump-thaw cycles. The internal pressure was evacuated to 10^{-3} mbar. The tube was sealed and placed in a preheated oven at 120 °C for 3 days. After finishing heating, the tube was cooled down and cut open. The formed yellow precipitate was filtered and washed with acetone/MeOH several times. Finally, the powder was dried in a normal oven at 80 °C. Yield = 92% (11 mg). Anal. Calcd (%):C, 71.28.; H, 4.32.; N, 13.85. Found (%): C, 70.92.; H, 4.42.; N, 13.27.

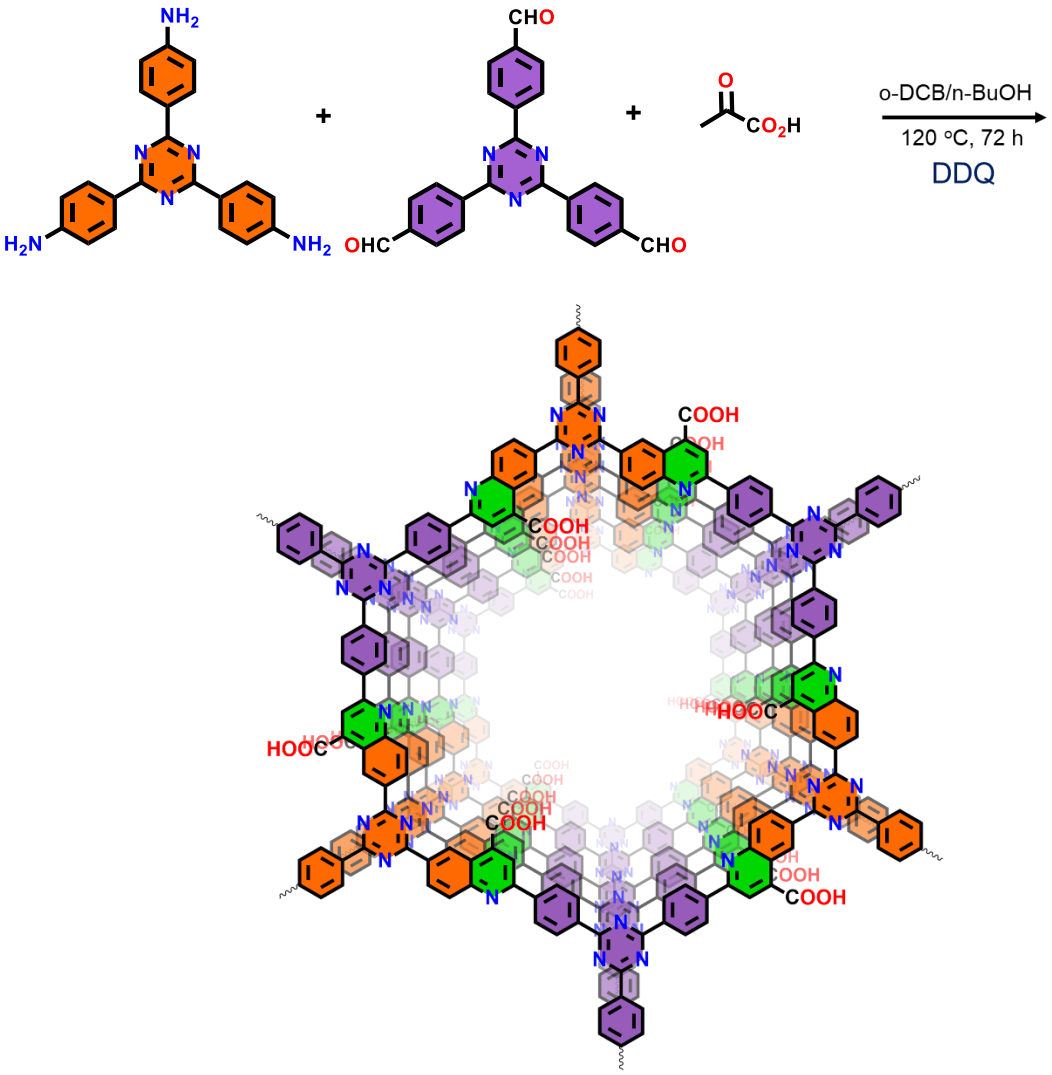

Scheme S2. Solvothermal synthesis of **DMCR-1.**

Synthesis of DMCR-1NH

A Pyrex glass tube (15 mL) was charged with 2,4,6-Tris(4-aminophenyl)triazine (Tta) (56 mg, 0.17 mmol), 4,4',4''-(1,3,5-triazine-2,4,6-triyl)tribenzaldehyde (Tta) (60 mg, 0.17 mmol), pyruvic acid (PA) (0.60 mmol, 60 μL), 1.5 mL *o*-DCB and 1.5 mL *n*-BuOH. The tube was first sonicated for 20 minutes and then flash frozen at 77 K (liquid N_2 bath) and degassed by three freeze-pump-thaw cycles. The internal pressure was evacuated to 10^{-3} mbar. The tube was sealed and placed in a preheated oven at 120 °C for 3 days. After finishing heating, the tube was cooled down and opened. The formed yellow precipitate was filtered and washed with acetone/MeOH several times. Finally, the powder was dried in a normal oven at 80 °C. Yield = 94.1% (118 mg). Anal. Calcd (%):C, 70.81.; H, 4.95.; N, 13.76. Found (%): C, 71.01.; H, 4.53.; N, 14.12.

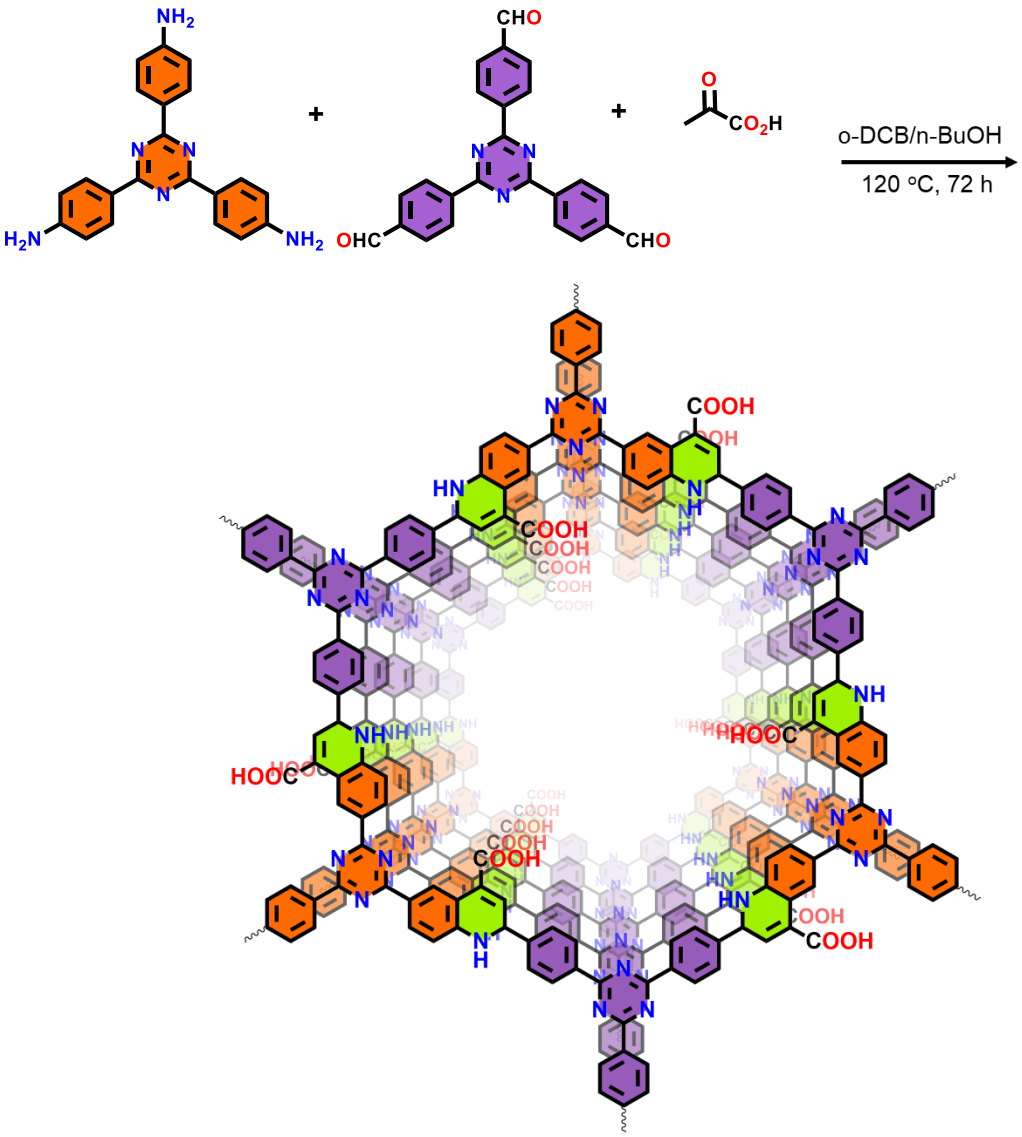

Scheme S3. Solvothermal synthesis of **DMCR-1NH**.

Solvothermal synthesis of Imine-1

A Pyrex glass tube (15 mL) was charged with 2,4,6-Tris(4-aminophenyl)triazine (Tat) (56 mg, 0.17 mmol), 4,4',4''-(1,3,5-triazine-2,4,6-triyl)tribenzaldehyde (Tta) (60 mg, 0.17 mmol), 1.5 mL *o*-DCB, 1.5 mL *n*-BuOH and 0.2 mL 6 M acetic acid aqueous solution. The tube was first sonicated for 20 minutes and then flash frozen at 77 K (liquid N_2 bath) and degassed by three freeze-pump-thaw cycles. The internal pressure was evacuated to 10^{-3} mbar. The tube was sealed and placed in a preheated oven at 120 °C for 3 days. After finishing heating, the tube was cooled down and opened. The formed yellow precipitate was filtered and washed with acetone/MeOH several times. Finally, the powder was dried in a normal oven at 80 °C. Yield = 82% (105 mg). Anal. Calcd (%):C, 76.57.; H, 4.75.; N, 17.86. Found (%): C, 75.55.; H, 4.12.; N, 17.02.

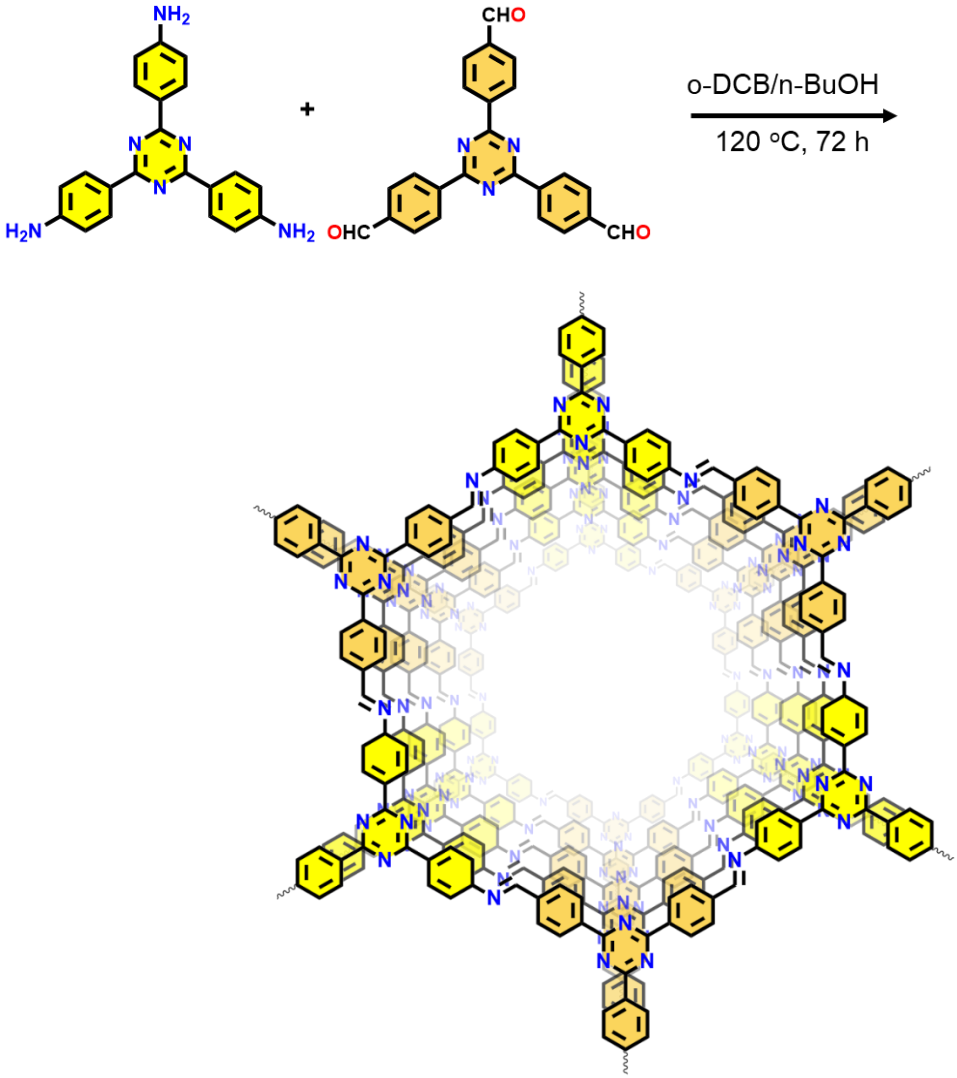

Scheme S4. Solvothermal synthesis of **Imine-1.**

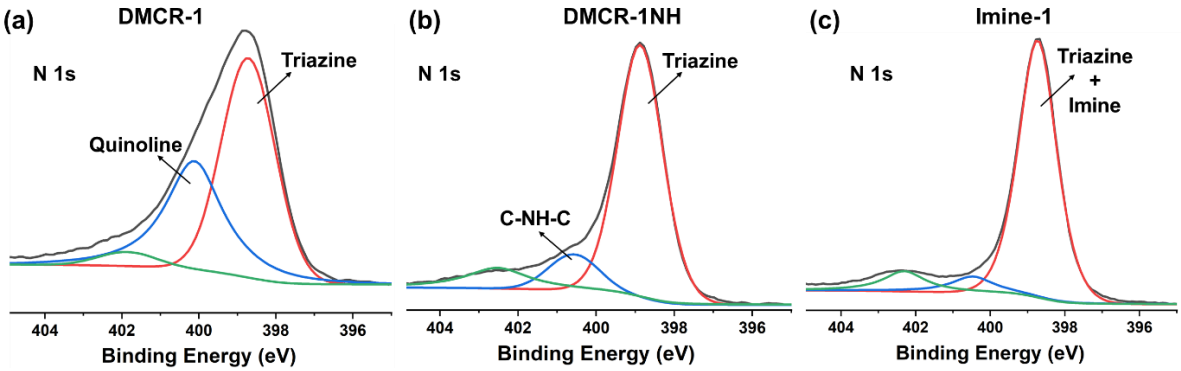

Figure S4. N(1s) XPS spectra of (a) **DMCR-1**, (b) **DMCR-1NH**, and (c) **Imine-1.**

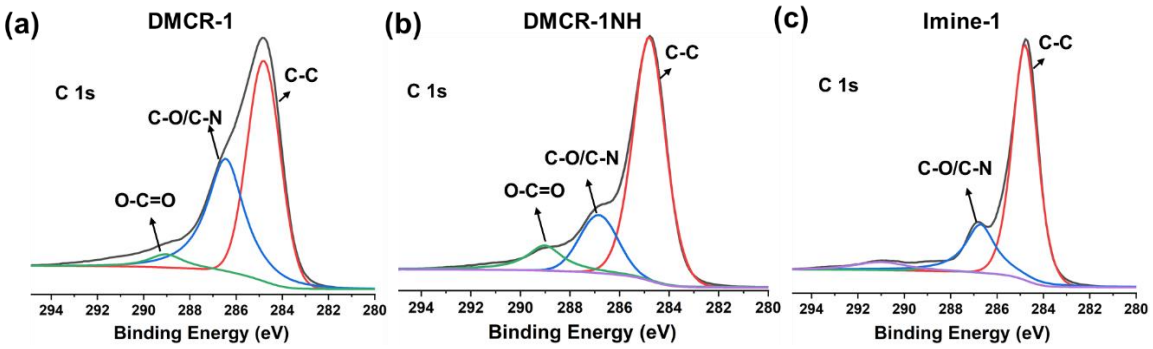

Figure S5. C(1s) XPS spectra of (a) **DMCR-1**, (b) **DMCR-1NH**, and (c) **Imine-1.**

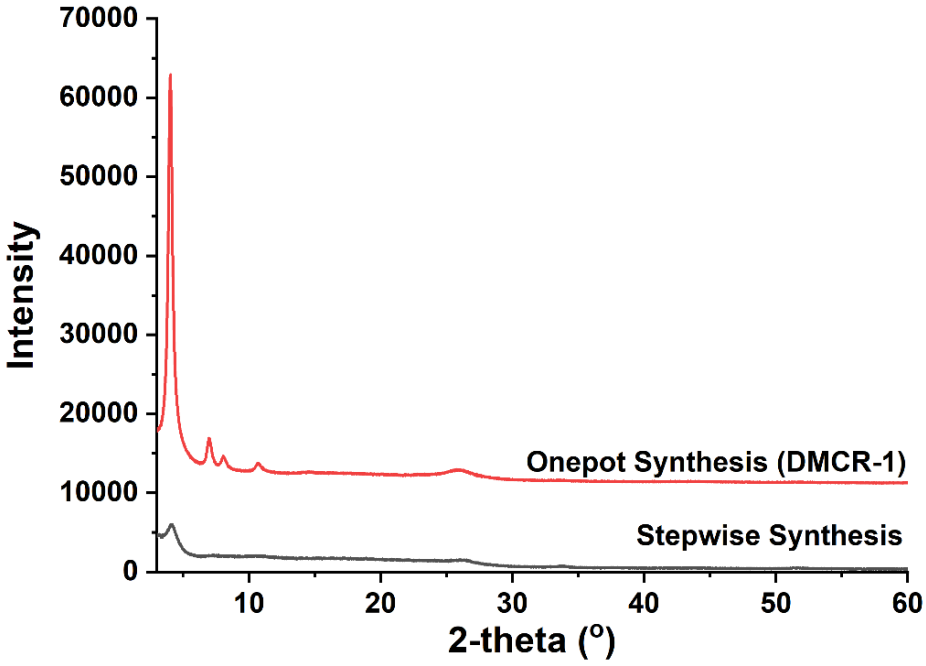

Figure S6. Comparison of experimental PXRD patterns of one-pot and stepwise synthesized **DMCR-1.**

Section S3. Structural Modelling and Atomic Coordinates of COFs

The structural crystal models with **hcb** topology of all the COFs were initially constructed in hexagonal unit cell in the Materials Studio suite of programs by Accelrys. Geometry optimization of the structures with Universal Force Field (UFF) led to satisfactory models whose theoretical pattern matched well the experimentally obtained patterns in terms of reflection positions and relative intensities. The Pawley profile refinements were performed using a Pseudo-Voigt profile function. The observed diffraction patterns were subjected to a polynomial background subtraction and the refined parameters included the zero-point shift, the unit cell parameters, the FWHM parameters and the peak asymmetry (Berar-Baldizzoni function). For all the COFs, AA stacking and AB stacking models were constructed, and their corresponding PXRD patterns were calculated. We chose to represent the AA structural model of the COFs in the fully eclipsed configuration (AA_e) except for **Imine-1** COF for which clear experimental observation of layer slippage can be deduced from the splitting of the lower symmetry reflections in the PXRD pattern. For **Imine-1** COF a model with slipped AA stacking (AA_s) in which the layers shift laterally by about 1.5 Å was constructed.

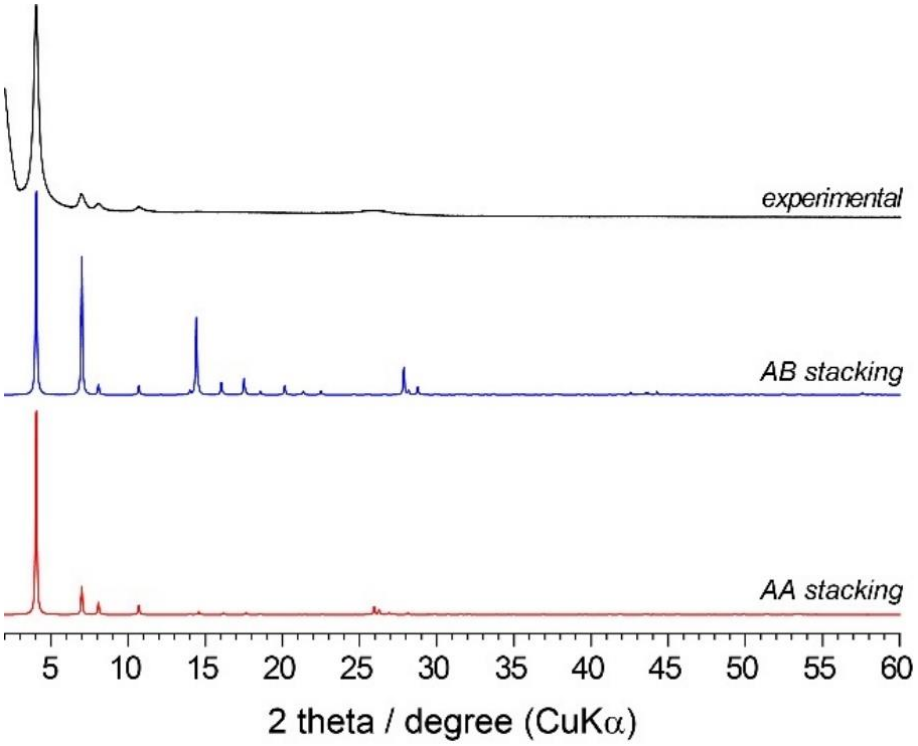

Figure S7. Simulated X-ray diffraction patterns for generated **hcb** hexagonal layered structures adopting fully eclipsed (red) and staggered (blue) stacking arrangement compared to the experimentally obtained pattern of **DMCR-1** (black).

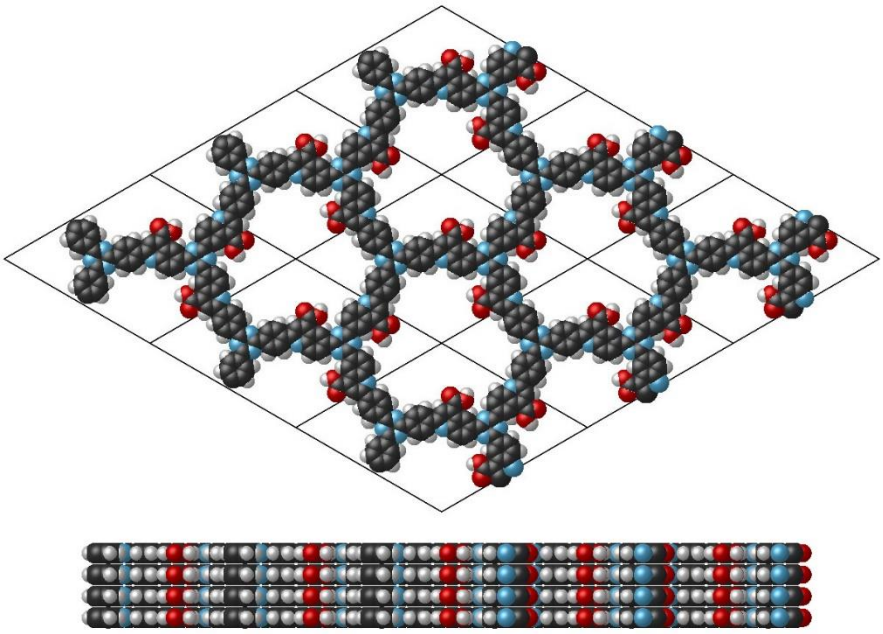

Figure S8. Simulated **hcb** 2D hexagonal layered model with eclipsed (AA) stacking arrangement of **DMCR-1**.

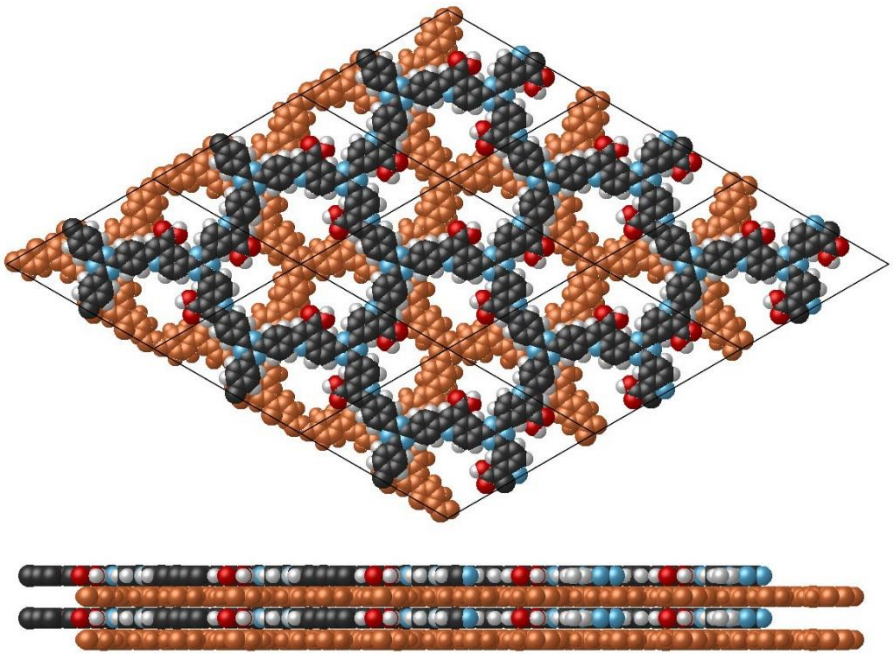

Figure S9. Simulated **hcb** 2D hexagonal layered model with staggered (AB) stacking arrangement of **DMCR-1**.

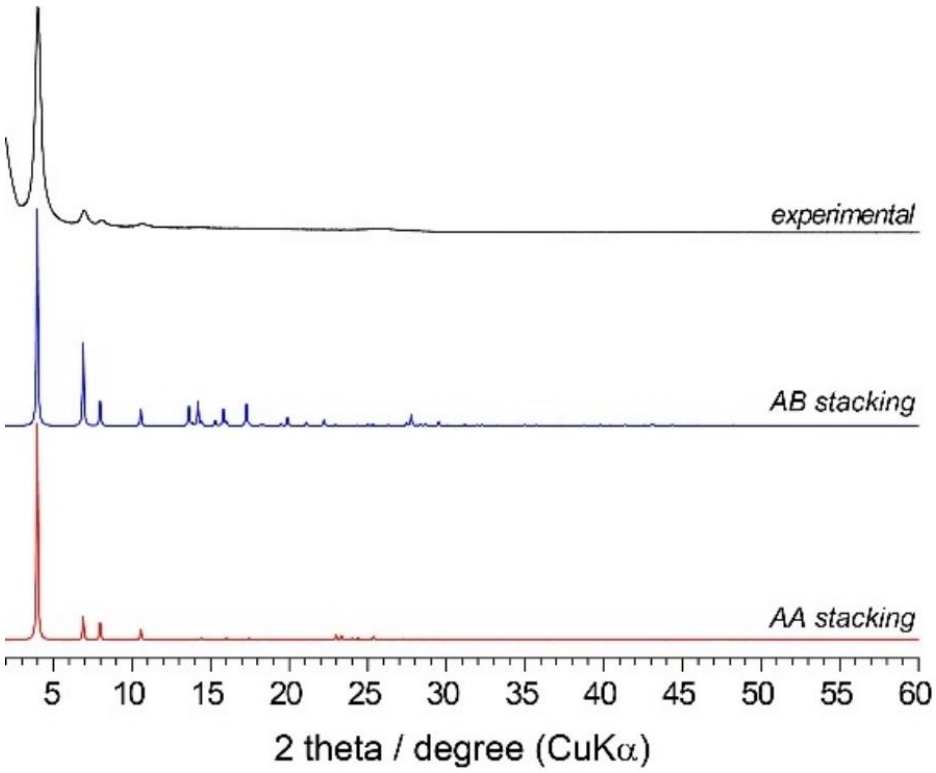

Figure S10. Simulated X-ray diffraction patterns for generated **hcb** hexagonal layered structures adopting fully eclipsed (red) and staggered (blue) stacking arrangement compared to the experimentally obtained pattern of **DMCR-1NH** (black).

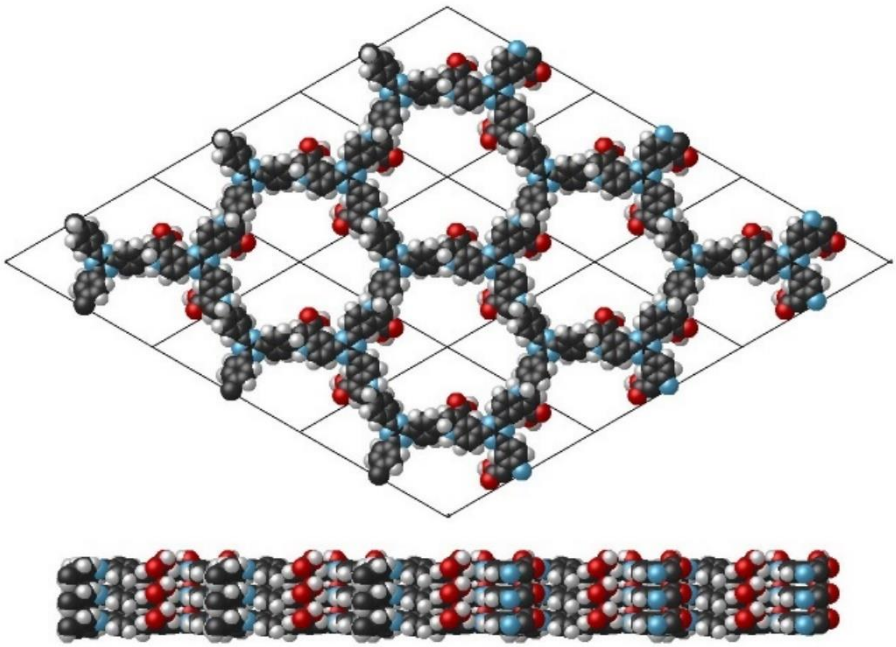

Figure S11. Simulated **hcb** 2D hexagonal layered model with eclipsed (AA) stacking arrangement of **DMCR-1NH**.

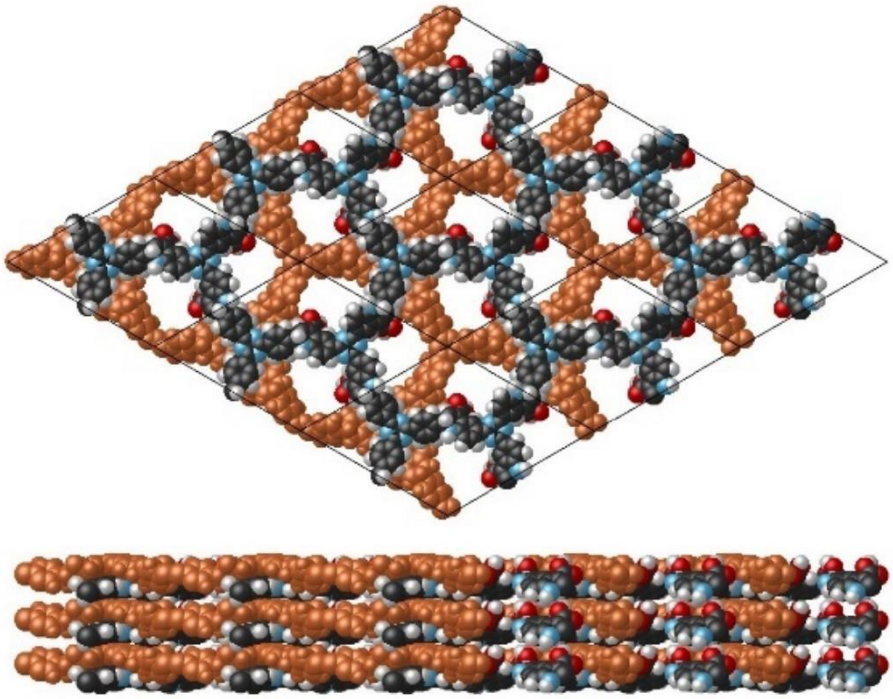

Figure S12. Simulated **hcb** 2D hexagonal layered model with staggered (AB) stacking arrangement of **DMCR-1NH**.

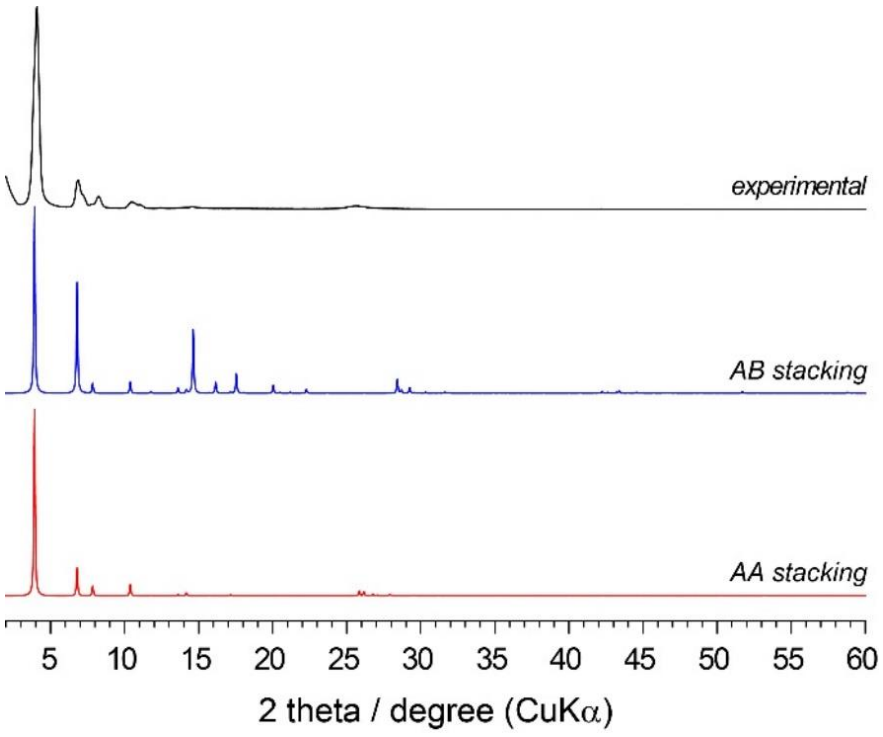

Figure S13. Simulated X-ray diffraction patterns for generated **hcb** hexagonal layered structures adopting fully eclipsed (red) and staggered (blue) stacking arrangement compared to the experimentally obtained pattern of **Imine-1** (black).

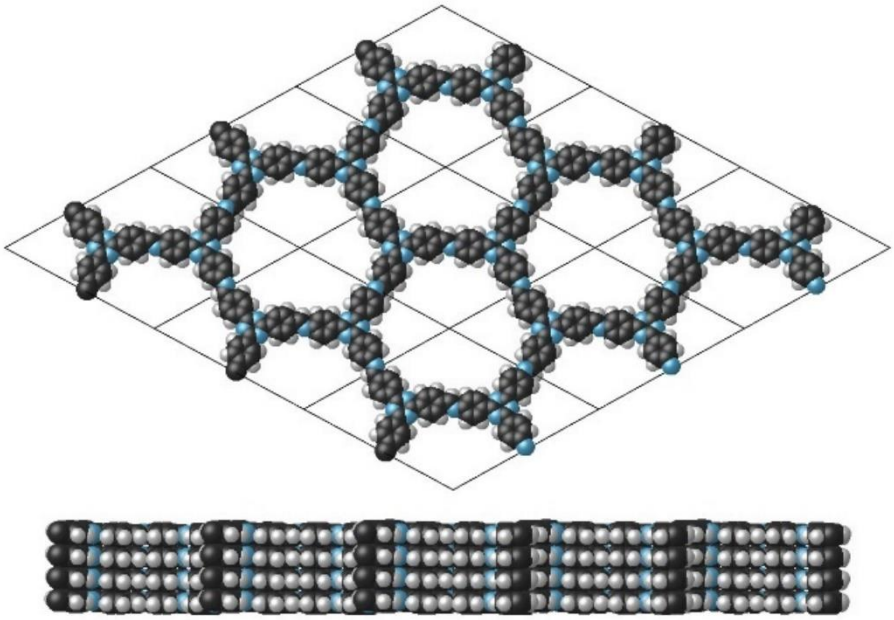

Figure S14. Simulated **hcb** 2D hexagonal layered model with eclipsed (AA) stacking arrangement of **Imine-1**.

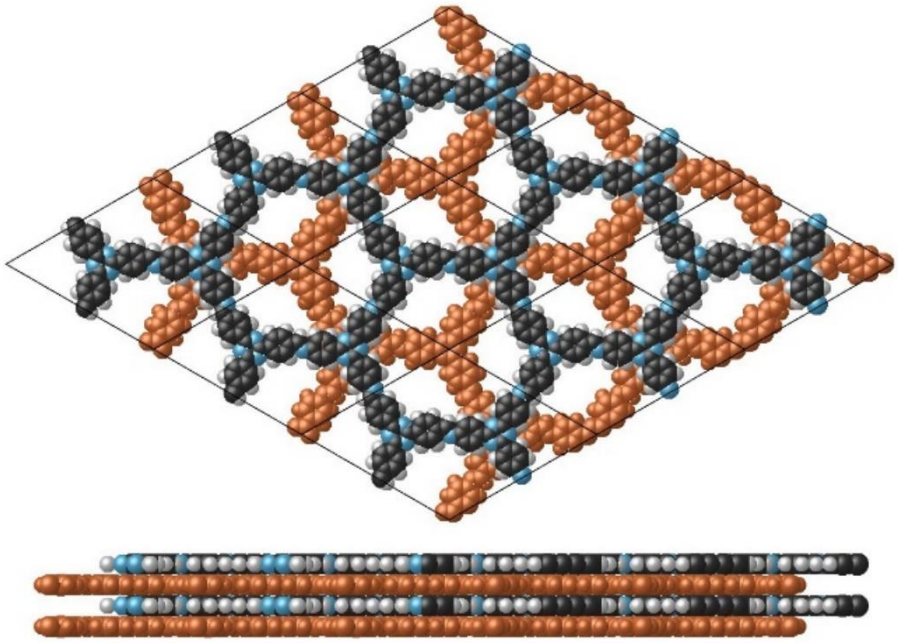

Figure S15. Simulated **hcb** 2D hexagonal layered model with staggered (AB) stacking arrangement of **Imine-1**.

Table S2. Fractional Atomic Coordinates for DMCR-1

DMCR-1				
Space Group: $P\bar{6}$ (174) a = 25.2864 Å, b = 25.2864 Å, c = 3.4327 Å $\alpha = \beta = 90.00$ °, $\gamma = 120.00$ °				
Atom label	**Atom type**	***x***	***y***	***z***
C1	C	0.27230	0.63587	0.00000
N2	N	0.30336	0.60615	0.00000
C3	C	-0.20755	-0.62090	0.00000
C4	C	-0.18431	-0.65980	0.00000
C5	C	-0.12256	-0.63745	0.00000
C6	C	-0.08200	-0.57521	0.00000
C7	C	-0.10584	-0.53654	0.00000
C8	C	-0.16756	-0.55899	0.00000
N9	N	0.01978	-0.48866	0.00000
C10	C	-0.01542	-0.54904	0.00000
C11	C	0.11064	-0.49347	0.00000
C12	C	0.08030	-0.46033	0.00000
C13	C	0.11195	-0.39786	0.00000
C14	C	0.17413	-0.36667	0.00000
C15	C	0.20590	-0.39759	0.00000
C16	C	0.17403	-0.46063	0.00000
H17	H	-0.21386	-0.70784	0.00000
H18	H	-0.10794	-0.66992	0.00000
H19	H	-0.07684	-0.48844	0.00000
H20	H	-0.18384	-0.52760	0.00000
H21	H	0.08814	-0.37320	0.00000
H22	H	0.19725	-0.31823	0.00000
H23	H	0.20028	-0.48209	0.00000
C24	C	0.64473	0.37168	0.00000
N25	N	0.60686	0.31157	0.00000
C26	C	0.58396	0.59633	0.00000
C27	C	0.55752	0.63290	0.00000
C28	C	0.59975	0.69946	0.00000
O29	O	0.58056	0.73922	0.00000
O30	O	0.65388	0.71890	0.00000
H31	H	0.60817	0.78193	0.00000
H32	H	0.63199	0.61748	0.00000

Table S3. Fractional Atomic Coordinates for DMCR-1NH

DMCR-1NH				
Space Group: *P*3 (143)				
a = 25.5305 Å, *b* = 25.5305 Å, *c* = 3.8637 Å				
$\alpha = \beta = 90.00$ °, $\gamma = 120.00$ °				
Atom label	**Atom type**	***x***	***y***	***z***
C1	C	0.27233	0.63940	-1.00544
N2	N	0.29987	0.60614	-1.00565
C3	C	0.64396	0.37106	0.05734
N4	N	0.60658	0.31076	0.05614
C5	C	-0.20763	-0.61928	-0.97451
C6	C	-0.18521	-0.65234	-1.14171
C7	C	-0.12391	-0.62669	-1.20590
C8	C	-0.08325	-0.56802	-1.09571
C9	C	-0.10573	-0.53610	-0.91235
C10	C	-0.16731	-0.56121	-0.85709
N11	N	0.01727	-0.47582	-1.12415
C12	C	-0.01776	-0.54008	-1.20270
C13	C	0.10760	-0.48167	-0.99772
C14	C	0.08045	-0.44696	-1.06161
C15	C	0.11541	-0.38445	-1.08232
C16	C	0.17761	-0.35623	-1.05451
C17	C	0.20603	-0.39024	-1.01303
C18	C	0.17065	-0.45296	-0.98662
H19	H	-0.21535	-0.69700	-1.23865
H20	H	-0.10833	-0.65209	-1.35262
H21	H	-0.07631	-0.49152	-0.81361
H22	H	-0.18346	-0.53516	-0.72239
H23	H	0.09447	-0.35762	-1.12785
H24	H	0.20345	-0.30787	-1.07608
H25	H	0.19266	-0.47916	-0.96750
C26	C	0.57443	0.58521	0.94388
C27	C	0.54799	0.61675	1.03924
C28	C	0.58576	0.67757	1.18995
O29	O	0.56201	0.70059	1.41032
O30	O	0.63926	0.70680	1.12030
H31	H	0.58596	0.74003	1.51071
H32	H	0.62263	0.60551	0.96756
H33	H	0.44880	0.44842	-0.20002
H34	H	0.54430	0.52667	-0.48532

Table S4. Fractional Atomic Coordinates for Imine-1

Imine-1				
Space Group: *P*1 (1) *a* = 26.1488 Å, *b* = 25.7622 Å, *c* = 3.4442 Å α = 79.92 °, β = 81.76 °, γ = 120.00 °				
C1	C	0.27088	0.64427	-0.06566
N2	N	0.30148	0.61445	-0.05521
C3	C	0.63941	0.37626	0.00198
N4	N	0.60257	0.31508	0.02055
C5	C	0.78627	0.38730	0.02435
C6	C	0.80850	0.34760	0.07785
C7	C	0.86955	0.37150	0.08114
C8	C	0.90952	0.43540	0.03361
C9	C	0.88750	0.47524	-0.02010
C10	C	0.82646	0.45139	-0.02358
N11	N	0.01756	0.51583	-0.07433
C12	C	0.97363	0.45934	0.04235
C13	C	0.11044	0.51328	-0.00694
C14	C	0.08073	0.54582	-0.06679
C15	C	0.11381	0.61042	-0.12133
C16	C	0.17551	0.64251	-0.12215
C17	C	0.20546	0.61032	-0.06544
C18	C	0.17224	0.54538	-0.00887
H19	H	0.77880	0.29799	0.11702
H20	H	0.88550	0.33990	0.12287
H21	H	0.91732	0.52481	-0.05829
H22	H	0.81088	0.48329	-0.06516
H23	H	0.98872	0.42709	0.06515
H24	H	0.08684	0.46336	0.04179
H25	H	0.09164	0.63612	-0.16644
H26	H	0.19970	0.69255	-0.16788
H27	H	0.19383	0.51910	0.03712
C28	C	0.36168	0.64549	-0.06065
N29	N	0.39116	0.70693	-0.07430
C30	C	0.62470	0.27722	0.03519
N31	N	0.68421	0.30100	0.03563
C32	C	0.61500	0.41732	-0.01649
C33	C	0.65448	0.48214	-0.08614
C34	C	0.63146	0.52088	-0.10471
C35	C	0.56857	0.49570	-0.05295
C36	C	0.52894	0.43092	0.01752
C37	C	0.55195	0.39217	0.03498

N38	N	0.48731	0.51548	-0.02433
C39	C	0.54544	0.53766	-0.07369
C40	C	0.48997	0.61535	-0.09979
C41	C	0.45792	0.55010	-0.03583
C42	C	0.39440	0.51688	0.01999
C43	C	0.36305	0.54767	0.01165
C44	C	0.39481	0.61273	-0.05192
C45	C	0.45861	0.64617	-0.10714
H46	H	0.70328	0.50310	-0.12753
H47	H	0.66288	0.57066	-0.15893
H48	H	0.48018	0.41013	0.05827
H49	H	0.52023	0.34246	0.08963
H50	H	0.57816	0.58707	-0.13088
H51	H	0.53889	0.64319	-0.14321
H52	H	0.36904	0.46672	0.06938
H53	H	0.31390	0.52038	0.05586
H54	H	0.48451	0.69634	-0.15702
C55	C	0.36107	0.73727	-0.08050
N56	N	0.30097	0.70563	-0.07726
C57	C	0.72158	0.36198	0.01955
N58	N	0.69890	0.39938	0.00067
C59	C	0.58443	0.21073	0.05066
C60	C	0.52122	0.18391	0.09821
C61	C	0.48320	0.12102	0.11663
C62	C	0.50762	0.08387	0.08311
C63	C	0.57080	0.11055	0.03433
C64	C	0.60880	0.17334	0.01795
N65	N	0.48872	0.99581	-0.10548
C66	C	0.46660	0.01774	0.09912
C67	C	0.39150	0.89710	-0.06726
C68	C	0.45490	0.93123	-0.10187
C69	C	0.48697	0.90135	-0.13480
C70	C	0.45665	0.83839	-0.12635
C71	C	0.39333	0.80403	-0.08901
C72	C	0.36113	0.83412	-0.05932
H73	H	0.50093	0.21132	0.12436
H74	H	0.43464	0.10144	0.15459
H75	H	0.59094	0.08299	0.00846
H76	H	0.65731	0.19255	-0.02081
H77	H	0.41795	-0.00126	0.16179
H78	H	0.36483	0.91819	-0.04744
H79	H	0.53577	0.92696	-0.16325
H80	H	0.48295	0.81679	-0.15039
H81	H	0.31233	0.80907	-0.03059

Section S4. FESEM and HRTEM Images, Surface Area and TGA of COFs

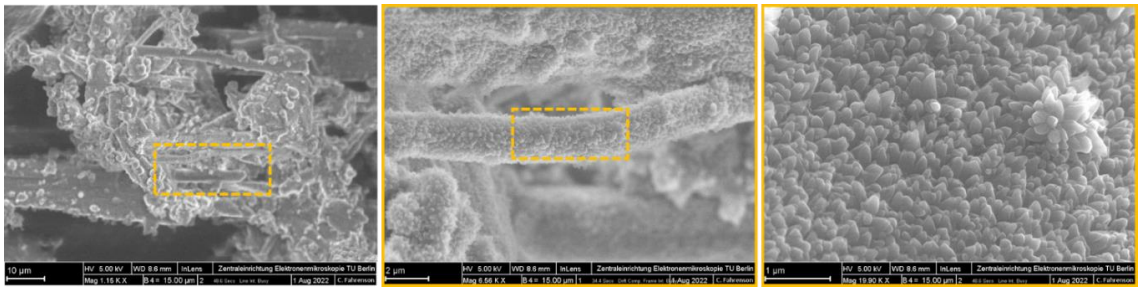

Figure S16. FESEM image of **DMCR-1**.

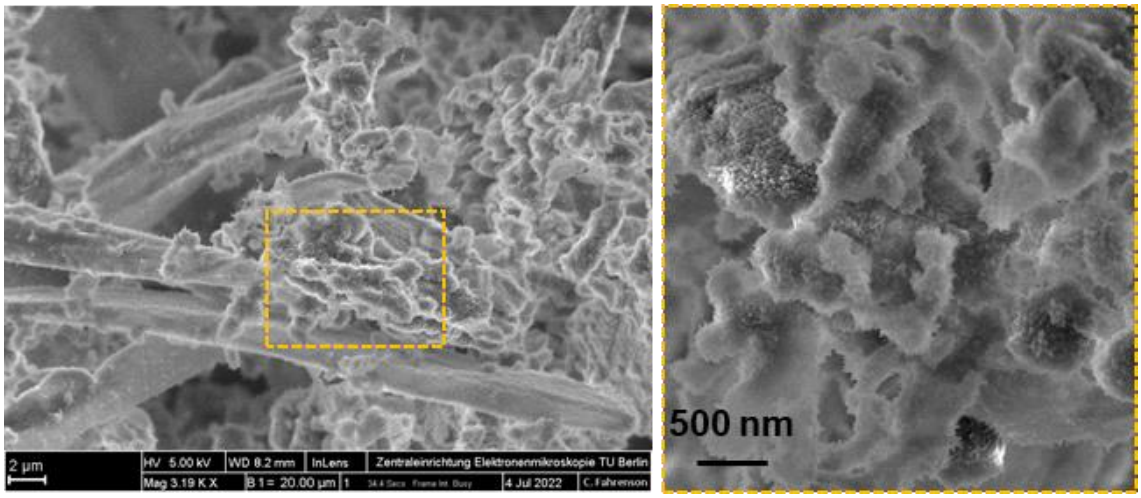

Figure S17. FESEM image of **DMCR-1NH**.

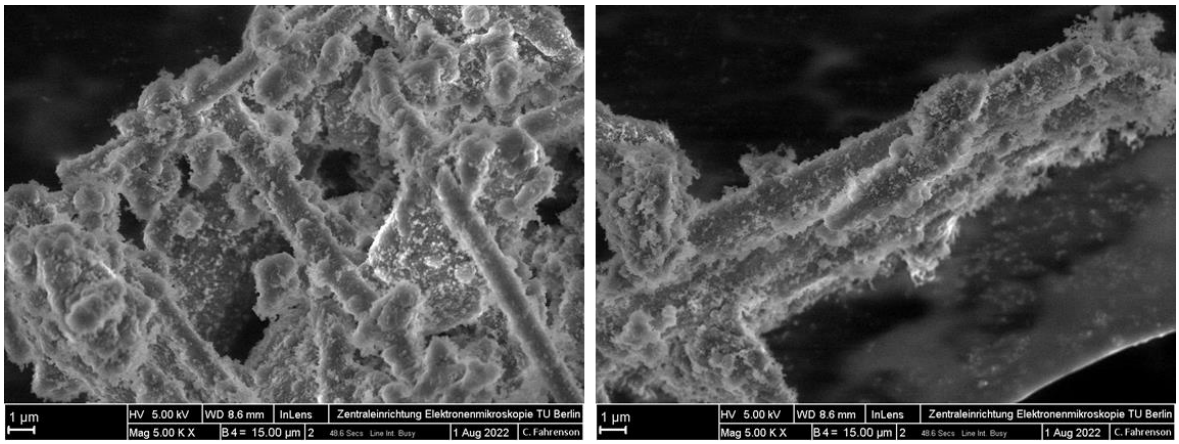

Figure S18. FESEM image of **Imine-1**.

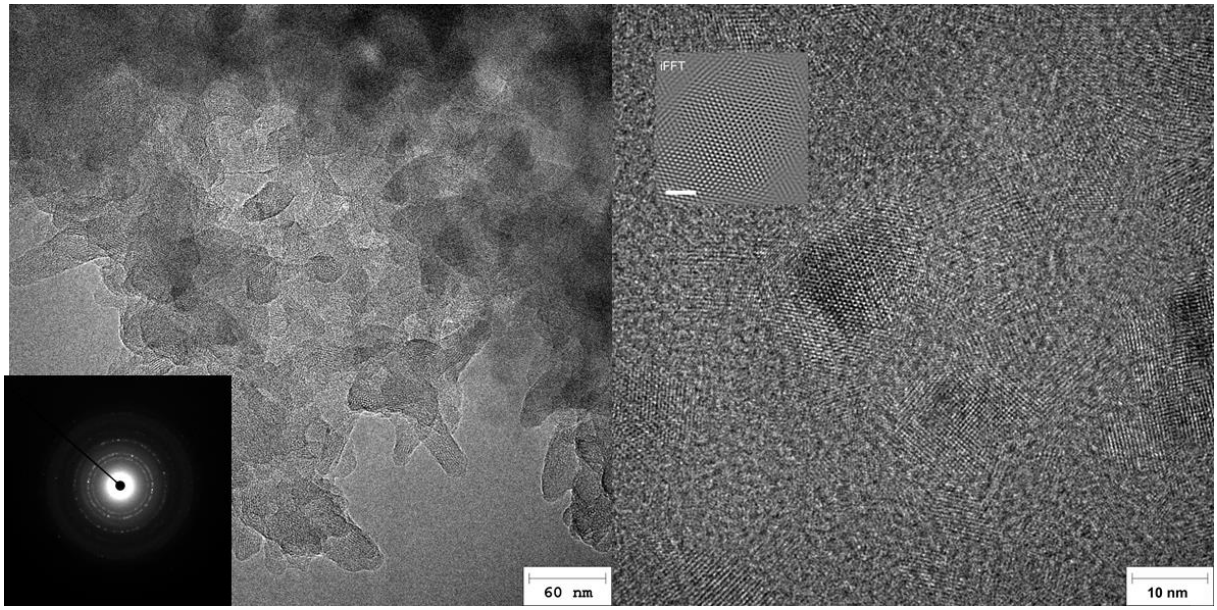

Figure S19. (Right) TEM image and (left) low dose HRTEM image of **DMCR-1**. Fast Fourier Transform (FFT) from the square on **DMCR-1.**

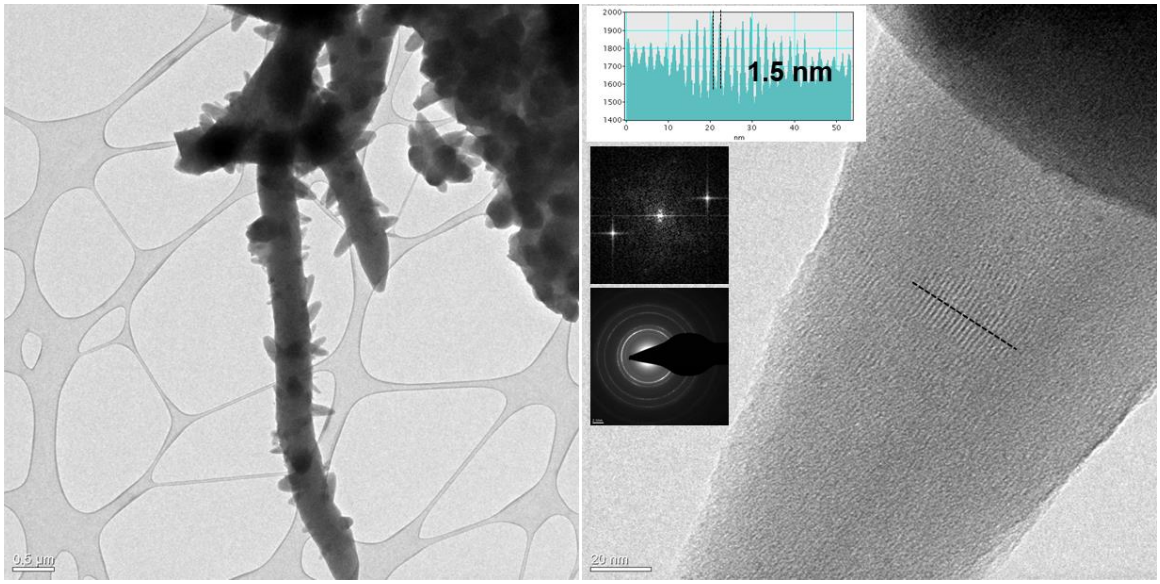

Figure S20. (Right) TEM image and (left) low dose HRTEM image of **DMCR-1NH**. Zoom image of nano rod showing ordered crystalline layers.

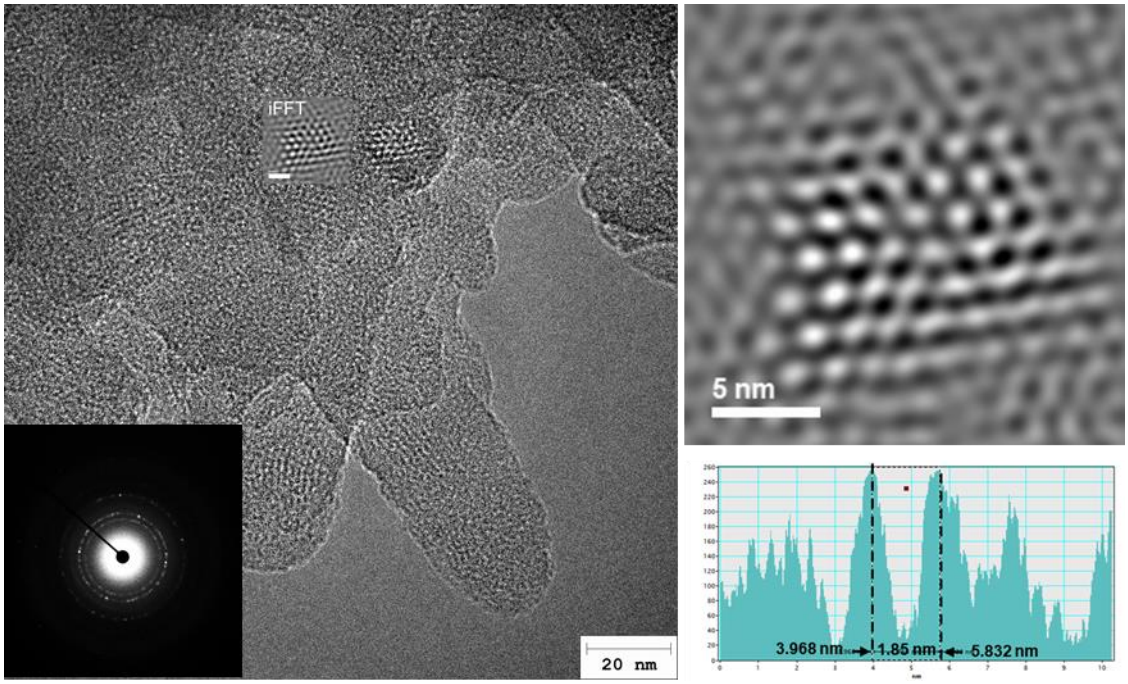

Figure S21. Low dose HRTEM image of **Imine-1**. A zoom on the nano rod shows a pore size of the COF (1.85 nm) close to the simulated structure.

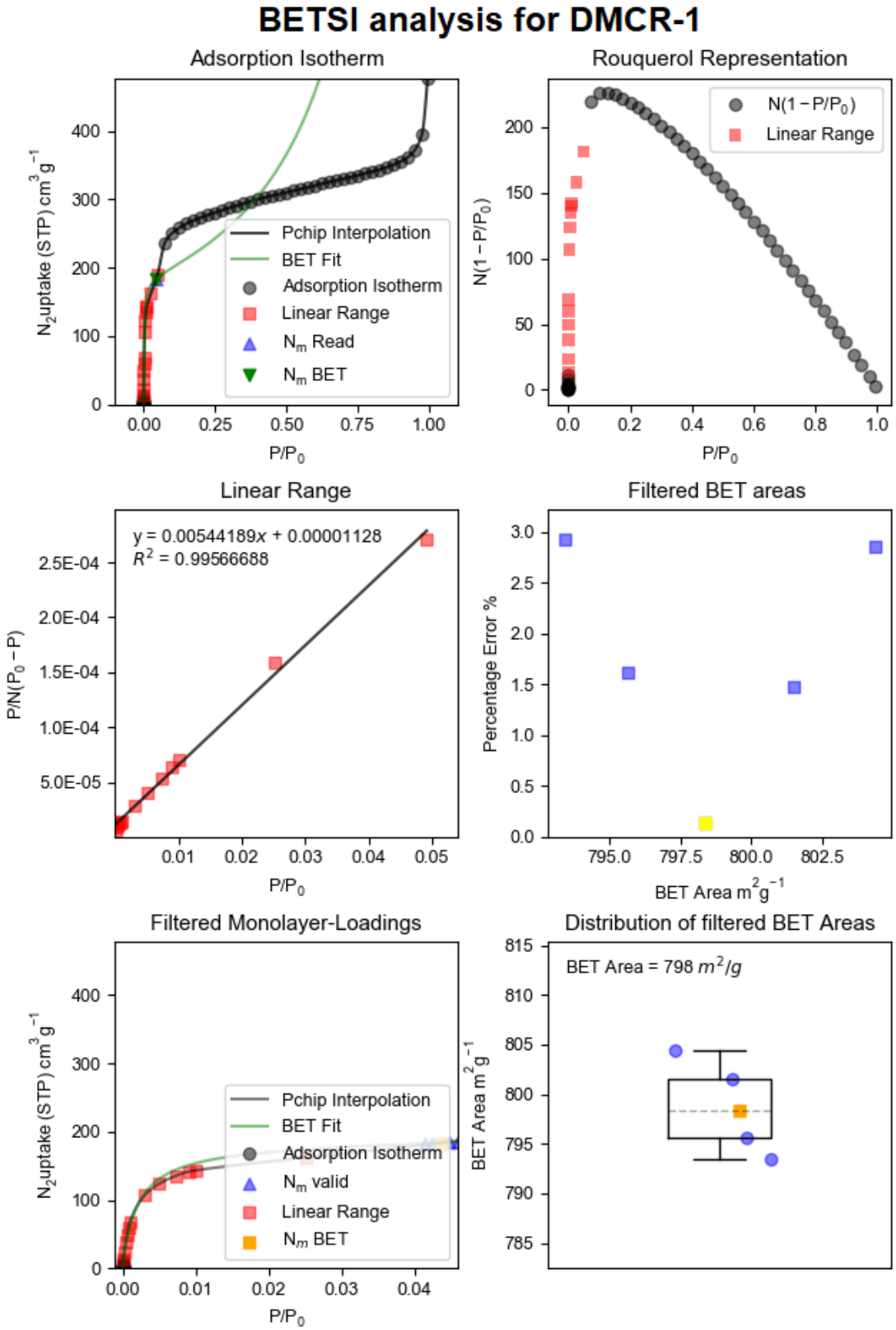

Figure S22. BET analysis of **DMCR-1** using the BETSI method.

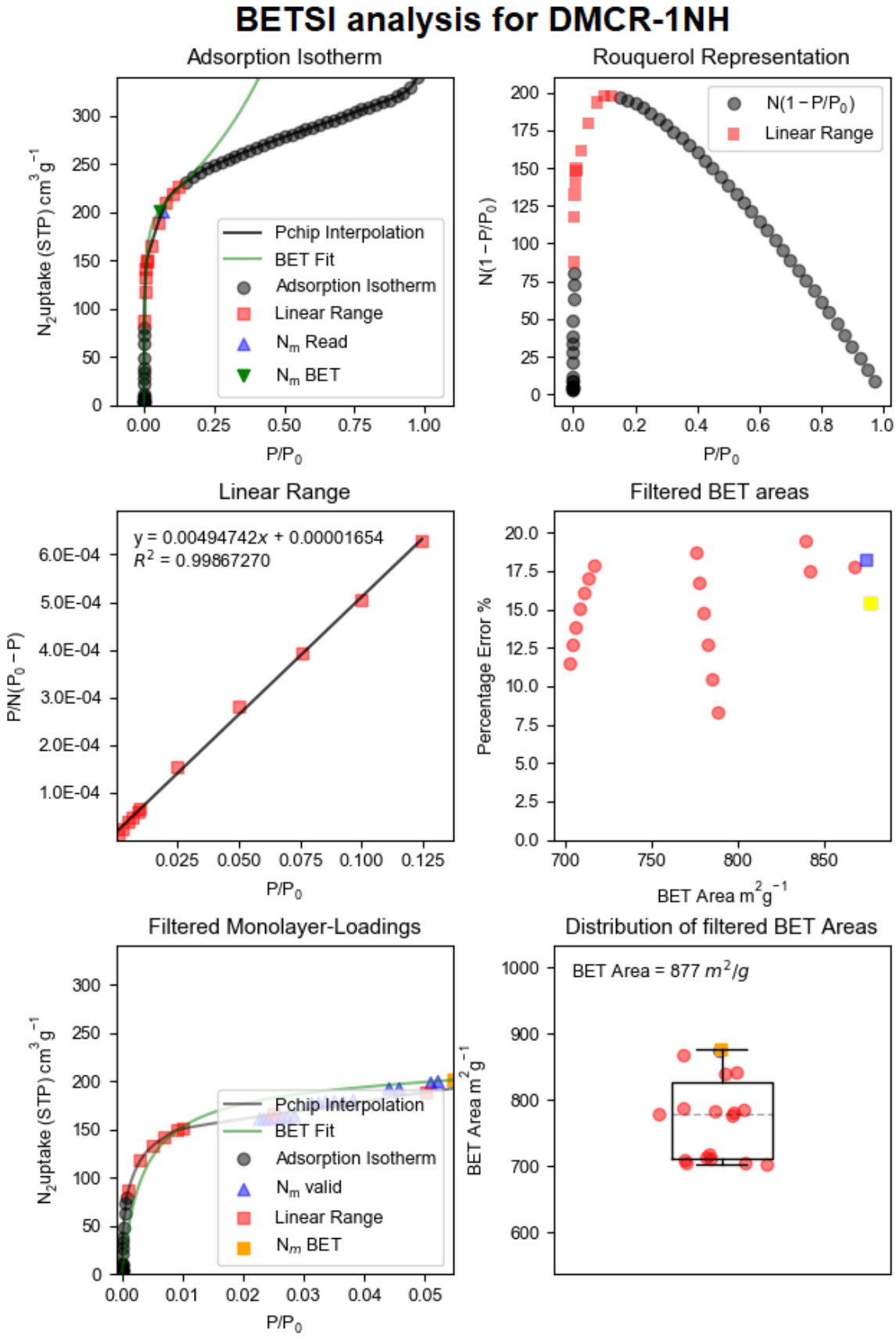

Figure S23. BET analysis of **DMCR-1NH** using the BETSI method.

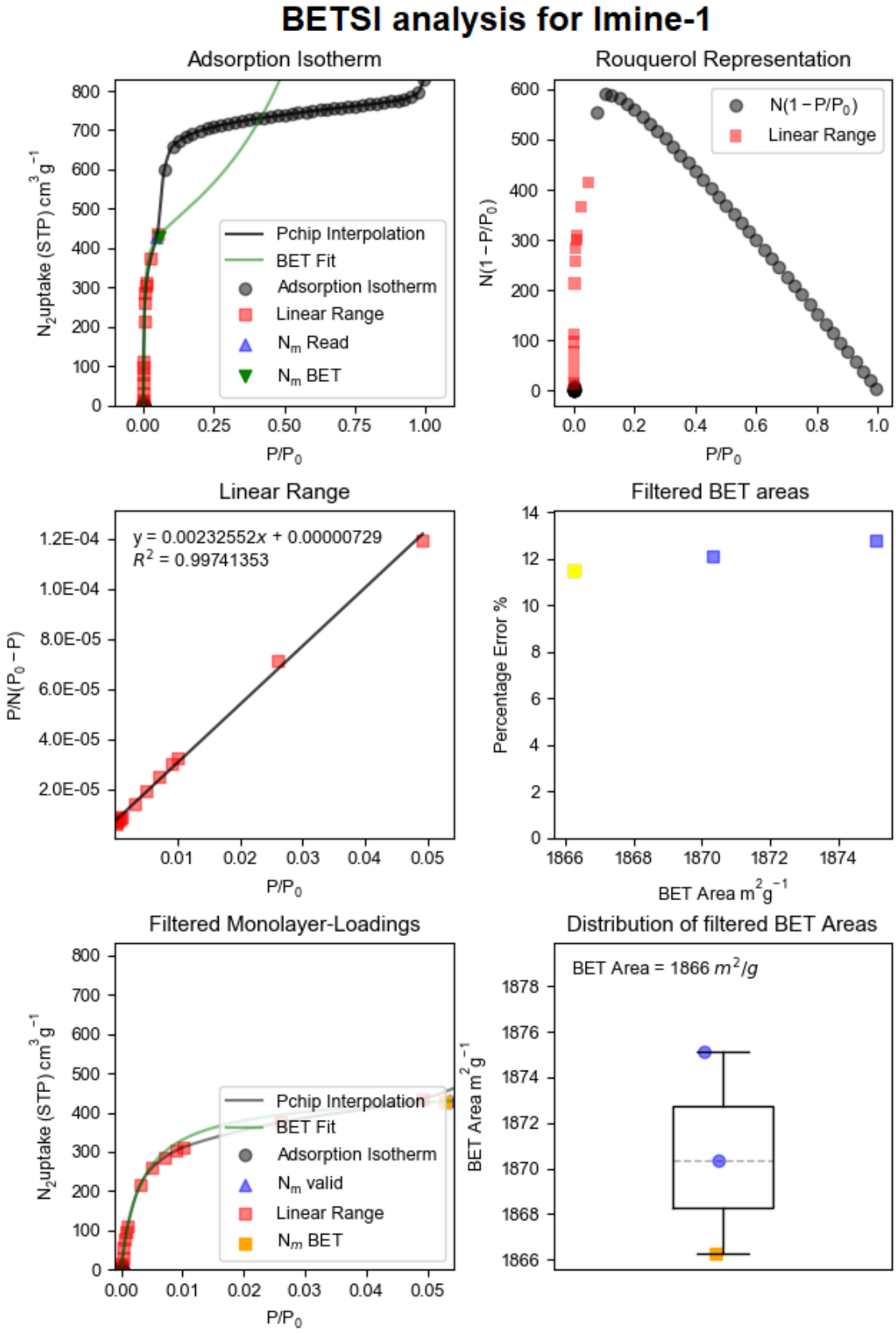

Figure S24. BET analysis of **Imine-1** using the BETSI method.

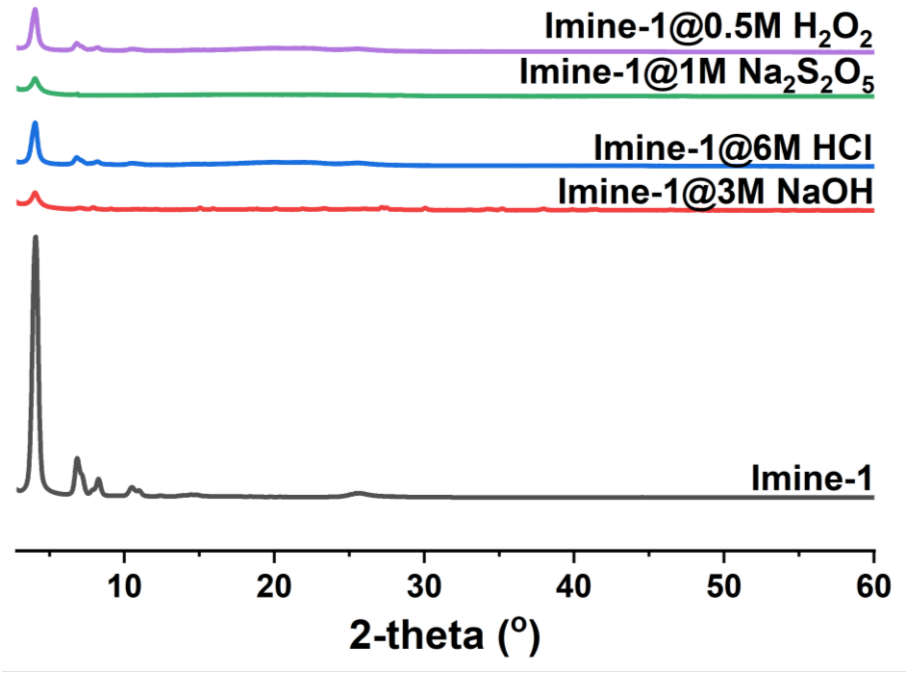

Figure S25. PXRD patterns collected for **Imine-1** after 1 day treatment with 6 M HCl, 3 M NaOH, 1 M $Na_2S_2O_5$ and 0.5 M H_2O_2.

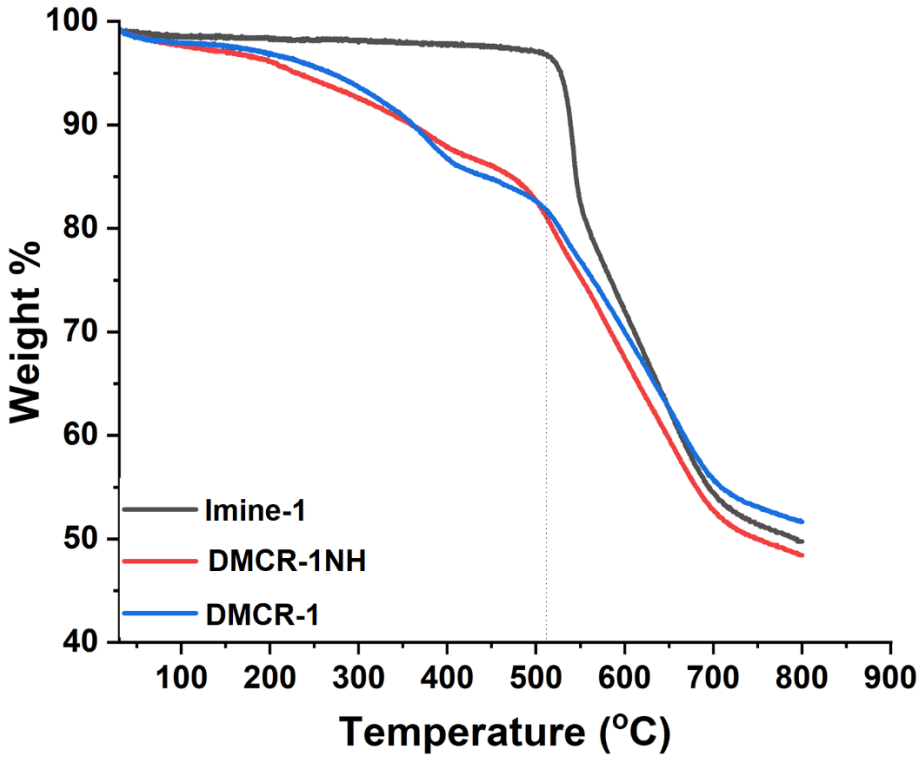

Figure S26. TGA of **DMCR** and **Imine** COFs. The weight loss from 150 to 400 ºC corresponds to the decomposition of the -COOH groups, not present in the imine-COF.

Section S5. UV-vis Spectra and Band Structure of COFs

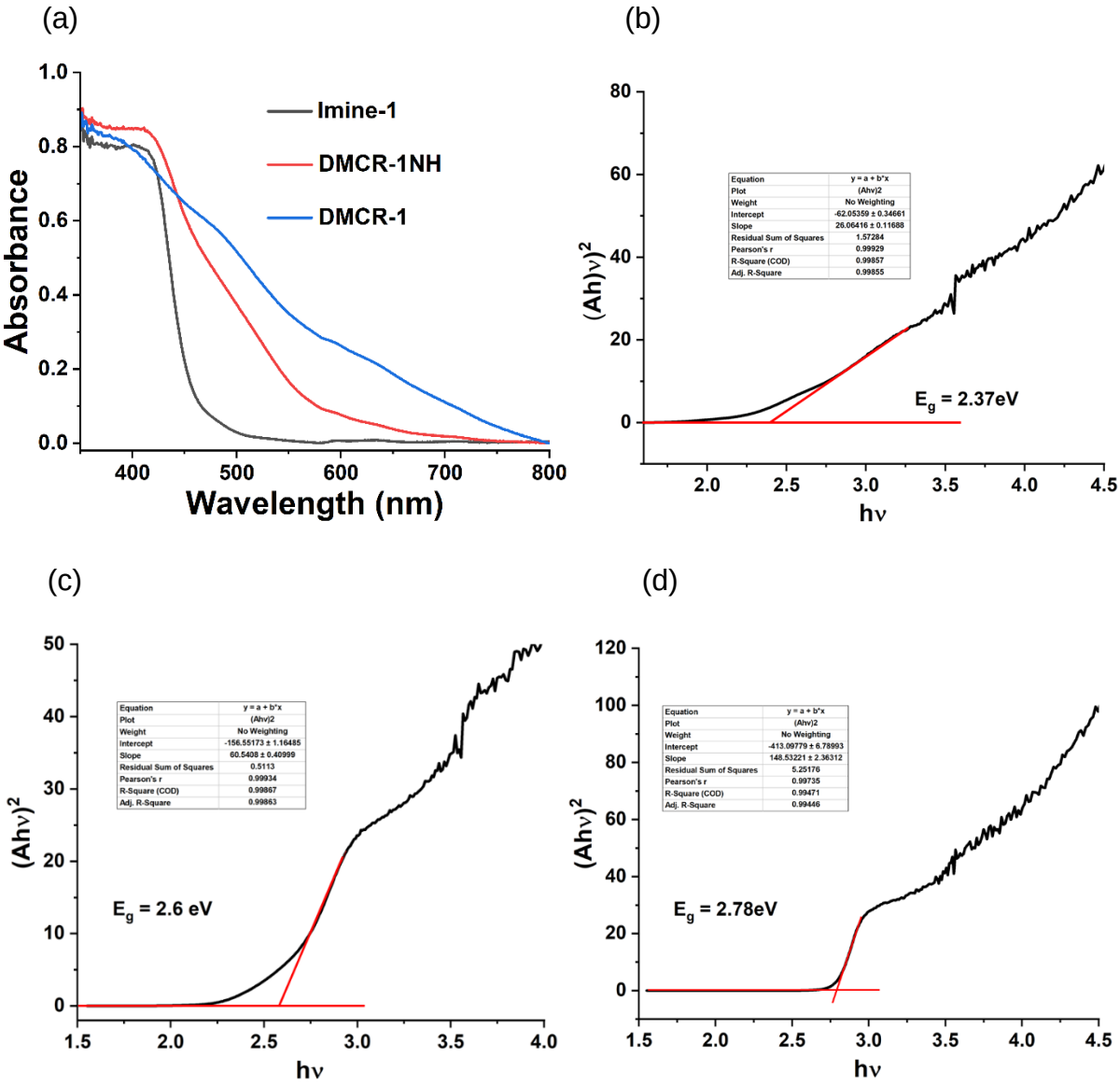

Figure S27. (a) Solid-state UV-vis spectra of **DMCR-1**, **DMCR-1NH** and **Imine-1**. Optical band gap calculation from the intersection of $(\alpha h\nu)^2$ vs $h\nu$ curve of (b) **DMCR-1**, (c) **DMCR-1NH** and (d) **Imine-1**.

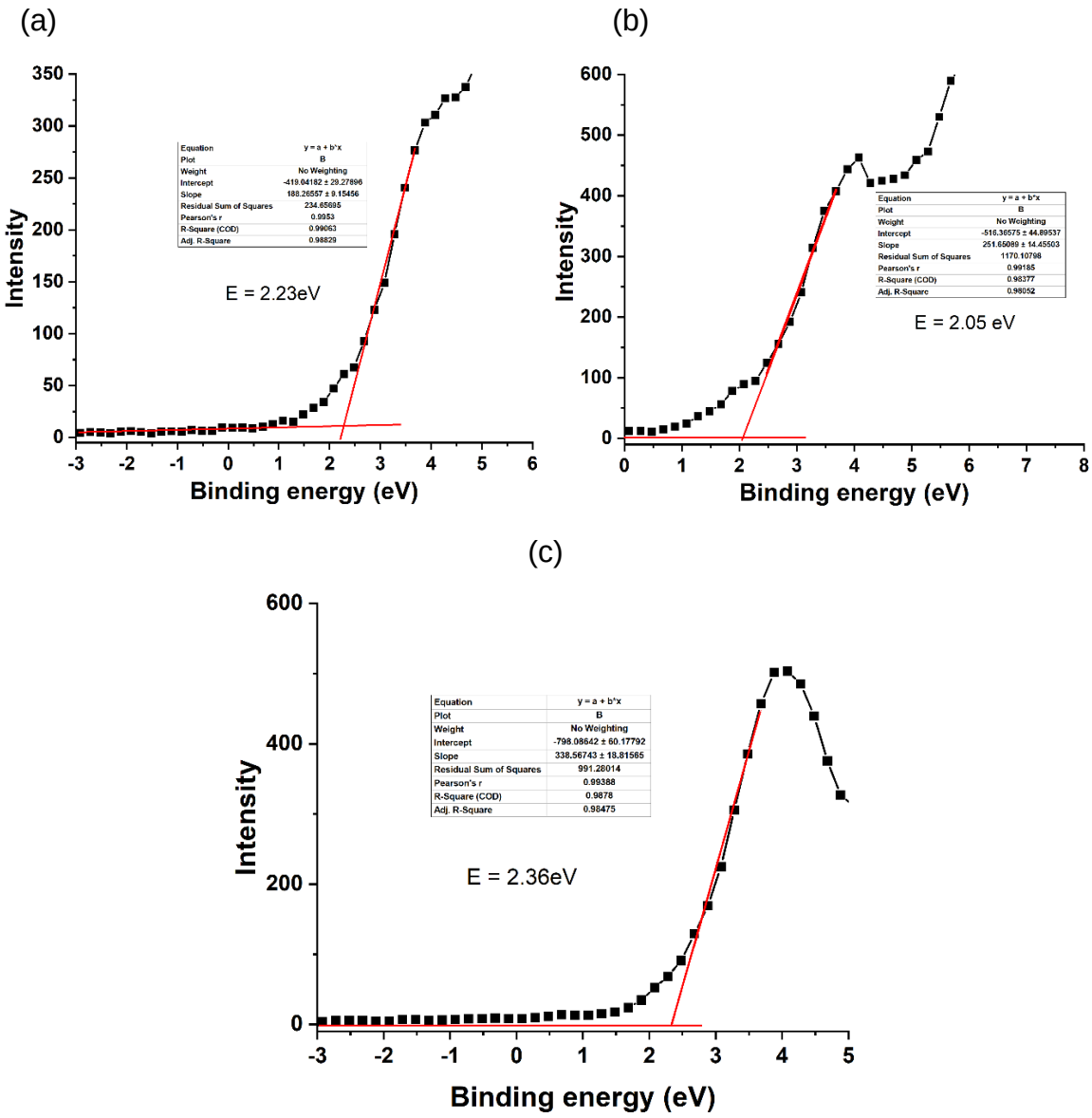

Figure S28. Valence band (VB) calculation from the VB XPS of (b) **DMCR-1**, (c) **DMCR-1NH** and (d) **Imine-1**.

Calculation of Valence band energy (E_{VB}) and conduction band energy (E_{CB})

$$E_{CB} = E_{VB} + E_g$$

$$E_{VB} = -(\varphi + VB_{xps})$$

E_g is the band gap derived from the UV-vis spectra, φ is the electron work function of the analyser (4.35 eV) and VB_{xps} is derived from valence band XPS spectra.

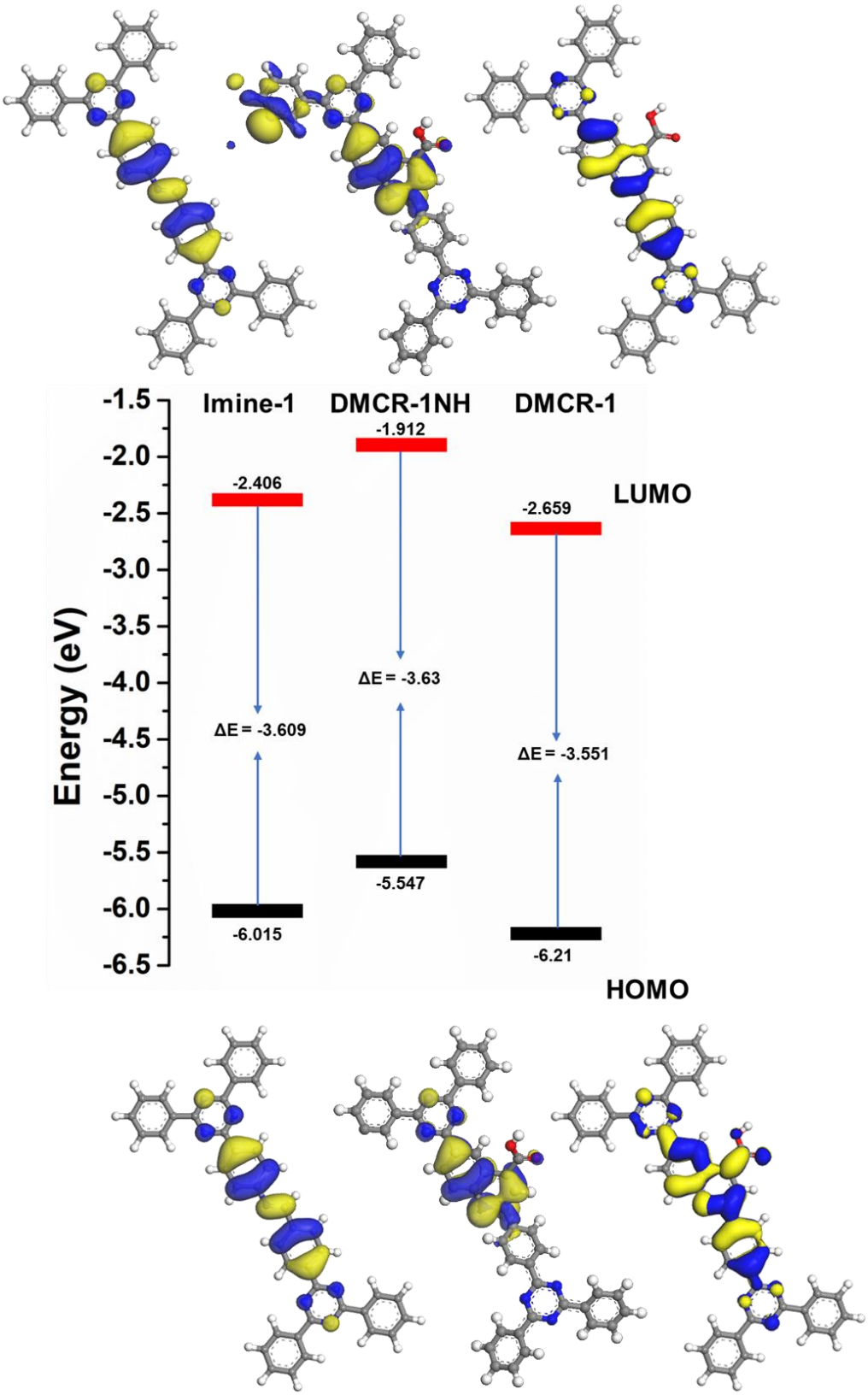

Figure S29. HOMO-LUMO energy profile calculated using the DFT method (basis set B3LYP/6-31G+(d)) showing frontier molecular orbital distribution of fragmented COFs.

Section 6. Photocatalytic Experiments

High-throughput Photocatalytic H_2O_2 Production Experiment

A sample vial was charged with COF powder (10 mg) in water (20 mL) without or with a sacrificial reagent (IPA, EtOH, BA or TBA) (2 mL), and then ultrasonicated for 10-15 min (to disperse the COF) after being capped under air. For oxygen atmosphere, the flask was purged for 10 min in each case. The photocatalytic H_2O_2 evolution experiments were performed on an Oriel Solar Simulator 300 W Xe lamp (L.O.T-Quantum design) with appropriate filters (420 nm). After 1h or 3h, 0.2 mL solution was taken by a syringe. The amount of H_2O_2 produced was analysed with Peroxide test sticks (HANNA Instruments, HI3844).

Photocatalytic Conversion Efficiency

AQY Measurement: The apparent quantum yield (AQY) was determined under monochromatic LED light irradiation at a certain wavelength (λ = 400 nm, 420 nm, 460 nm, 490 nm, 550 nm, and 600 nm), and the light intensity was measured by a ThorLabs PM100D Power with a photodiode sensor. The AQY was calculated using the following equation:

$$AQY\ \% = \frac{[H_2O_2\ \text{produce (mol)}]\ \text{x}\ 2}{\text{Photon number entered into the reactor (mol)}}\ \text{x}\ 100$$

$$= \frac{[\text{Na x h x c}]\ \text{x}\ [H_2O_2\ \text{produce (mol)}]\ \text{x}\ 2}{\text{I x S x t x}\ \lambda}\ \text{x}\ 100$$

Where, ***Na*** is Avogadro's constant (6.022×10^{23} mol^{-1}), ***h*** is the Planck constant (6.626 × 10-34 Js), ***c*** is the speed of light (3×10^8 ms^{-1}), ***S*** is the irradiation area (cm^2), ***I*** is the intensity of irradiation light (Wcm^{-2}), ***t*** is the photoreaction time (s), ***λ*** is the wavelength of the monochromatic light (m).

Electron Paramagnetic Resonance Measurements

Spin trapping electron paramagnetic resonance (EPR) measurements were performed using a an ESR spectrometer (Bruker-BioSpin, EMXmicro). 5,5-dimethyl-1-pyrroline N-oxide (DMPO) were used as a spin-trapping reagent to detect radicals. The measurements were carried out in a H_2O/MeOH (1:9, 500 μL): mixture with 2 mg of COFs and 0.1 mmol DMPO, a Xe lamp with a filter (λ > 420 nm) was applied as the light source.

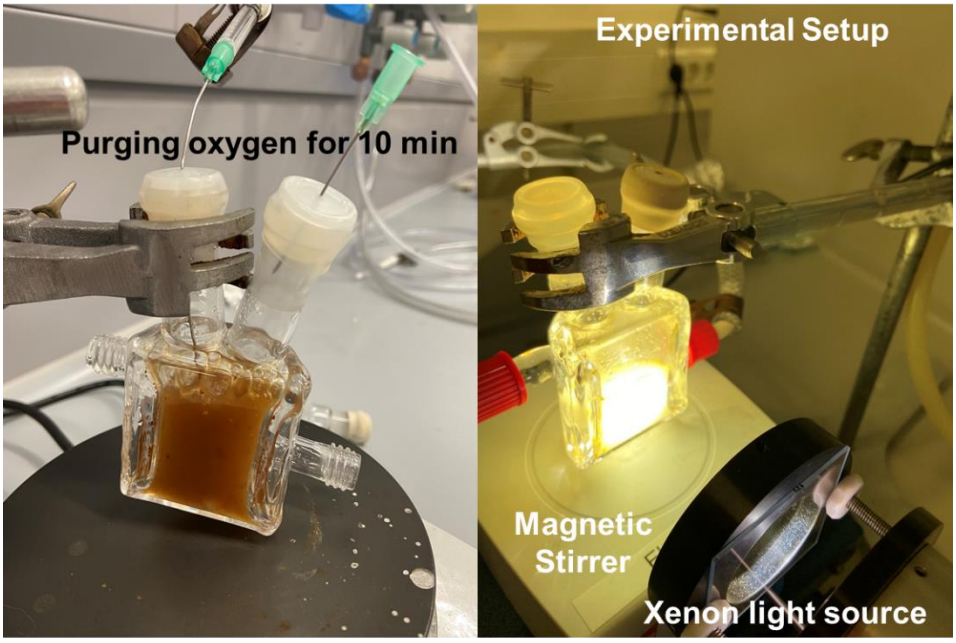

Figure S30. Experimental setup for photocatalytic H_2O_2 formation: (left: O_2 purging.; right: experiment on progress).

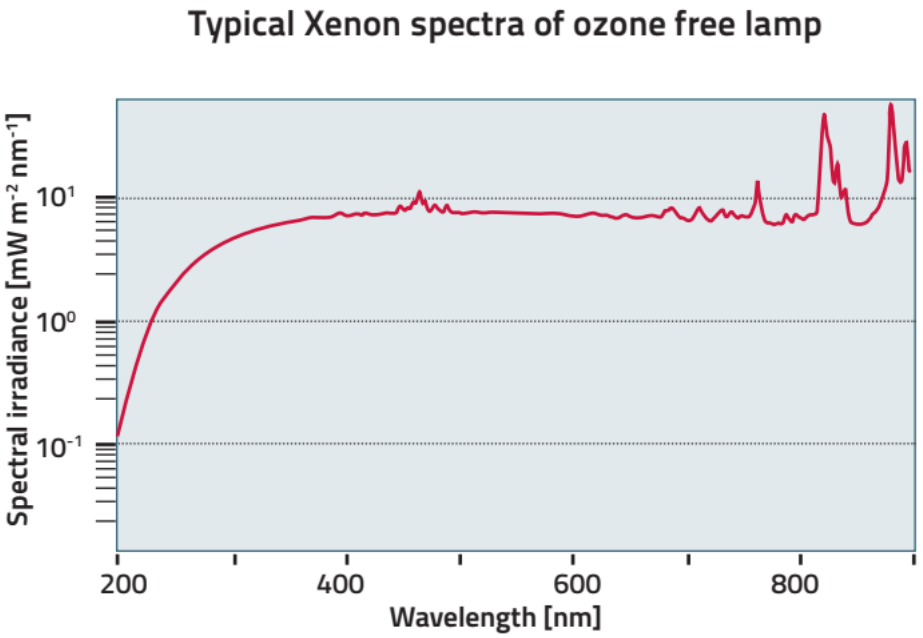

Figure S31. Xenon lamp light spectra used for this experiment.

https://qdeurope.com/fileadmin/Mediapool/products/lightsources/en/Xenon_arc_light_sources_300_W.pdf

https://qdeurope.com/fileadmin/Mediapool/products/lightsources/en/Lamp_spectra_and_irradiance.pdf

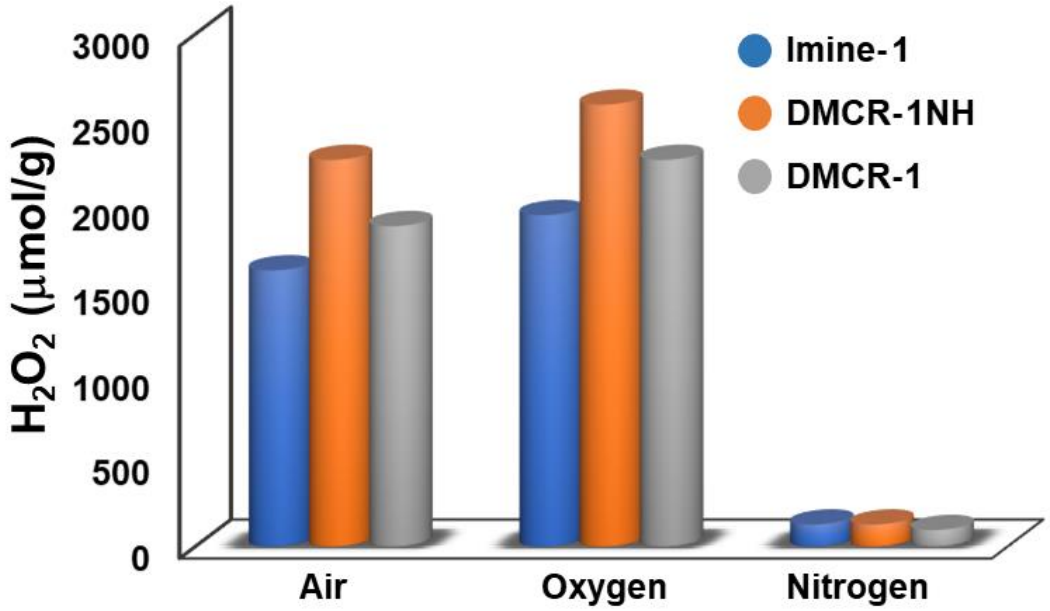

Figure S32. Photochemical H_2O_2 production under different gas atmosphere (5 mg of COFs in 11 mL water, 1 h at 25 ^{o}C and λ = 420 nm).

Photocurrent Measurement.

Photocurrent measurements are performed with a three-electrode set-up from Metrohm (Autolab PGSTAT302N), using a Pt counter electrode, an Ag/AgCl (3 M NaCl) reference electrode and $NaSO_4$ (2 M in water) as electrolyte. The working electrode was fabricated by mixing under sonication 5 mg COFs with water, ethanol (50 µL each) and 1 wt% Nafion solution for 30 mins. Then, 2 µL of the suspension was drop-casted onto 0.25 cm^2 of a FTO substrate and dried under ambient conditions. Spare FTO surface was covered with an isolating paint. Photocurrent measurements were performed at 1 V bias under periodical illumination from the back (40 s intervals, visible light, 1 W m^{-2}).

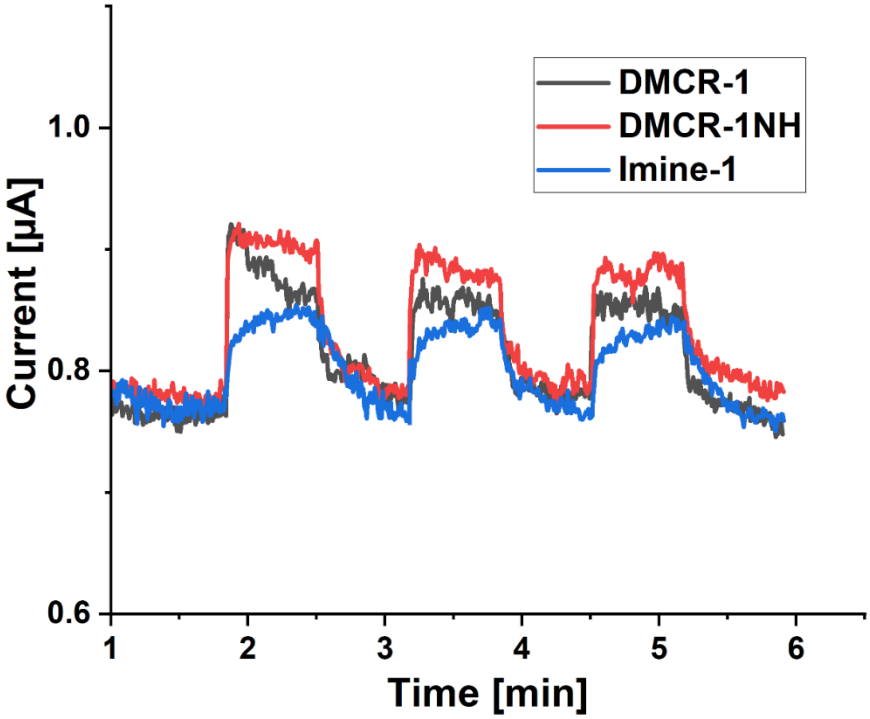

Figure S33. Photocurrent spectra of **DMCR-1**, **DMCR-1NH**, **Imine-1** with and without visible light irradiation.

Solid-State Electron Paramagnetic Resonance Spectroscopy (EPR)

EPR measurements in X-band (microwave frequency ≈ 9.87 GHz) were performed at 293 K by a Bruker EMX CW micro spectrometer equipped with an ER 4119HS-WI high-sensitivity optical resonator with a grid on the front side. The samples were illuminated by a 300 W Xe lamp with a 420 nm cut-off filter (LOT Oriel). All the samples were measured under the same conditions (microwave power: 6.74 mW, modulation frequency: 100 kHz, modulation amplitude: 3 G, Sweep time: 45 s). g values have been calculated from the resonance field B_0 and the resonance frequency v using the resonance condition $hv = g\beta B_0$. The calibration of the 3 g values was performed using DPPH (2, 2-diphenyl-1- picrylhydrazyl) (g = 2.0036 ± 0.00004).

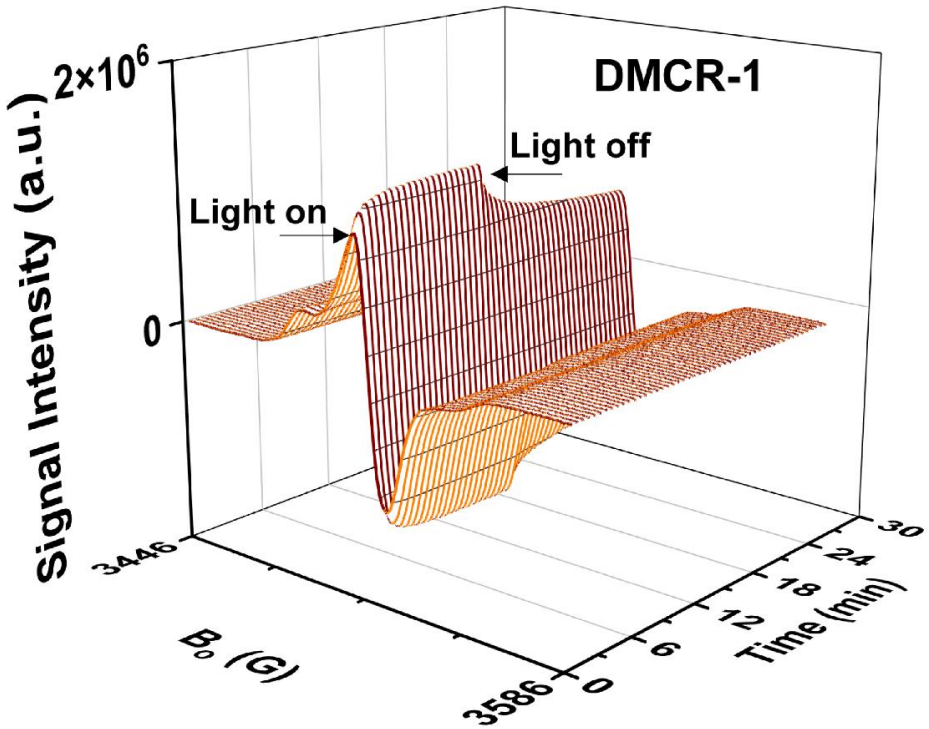

Figure S34. Electron paramagnetic resonance (EPR) conduction band (CB) electrons spectra of **DMCR-1** with and without visible light irradiation (>420 nm, 300 W Xe lamp).

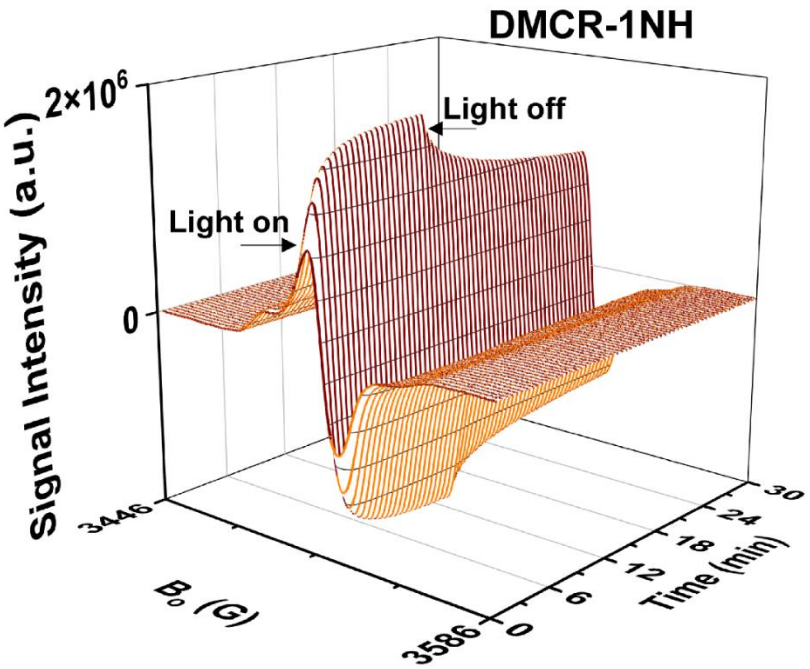

Figure S35. Electron paramagnetic resonance (EPR) conduction band (CB) electrons spectra of **DMCR-1NH** with and without visible light irradiation (>420 nm, 300 W Xe lamp).

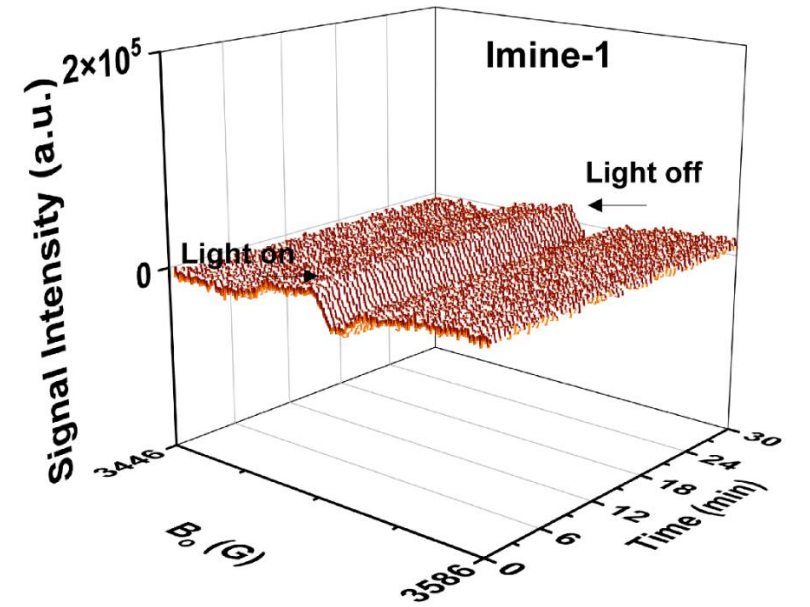

Figure S36. Electron paramagnetic resonance (EPR) conduction band (CB) electrons spectra of **Imine-1** with and without visible light irradiation (>420 nm, 300 W Xe lamp).

Section 7. Configurational Bias Monte Carlo simulation

Configurational Bias Monte Carlo (CBMC) molecular simulation:

The structures of **DMCR-1**, **DMCR-1NH** and **Imine-1** was assumed to be rigid in the crystallographic position, which is obtained from Pawley refinement PXRD data. The simulation boxes representing **DMCR-1**, **DMCR-1NH** and **Imine-1** adsorbent consist of (1 x 1 x 1) unit cells for O_2. All the calculations were performed at 298 K. Interatomic interactions were modeled with standard Lennard-Jones potential and Columbic potentials. Lennard-Jones parameters between unlike atom types were computed using the Lorentz-Berthelot mixing rules. The pairwise interactions between host guest atoms of the particular force field, nonbonding parameter has been utilized. The long-range part of electrostatic interactions was handled using the Ewald summation technique with a relative precision of 10^{-6}. Periodic boundary conditions were applied in all three dimensions. For each state point, the CBMC simulation consists of 1×10^7 steps to guarantee equilibration, followed by 1×10^7 steps to sample the desired thermodynamic properties.

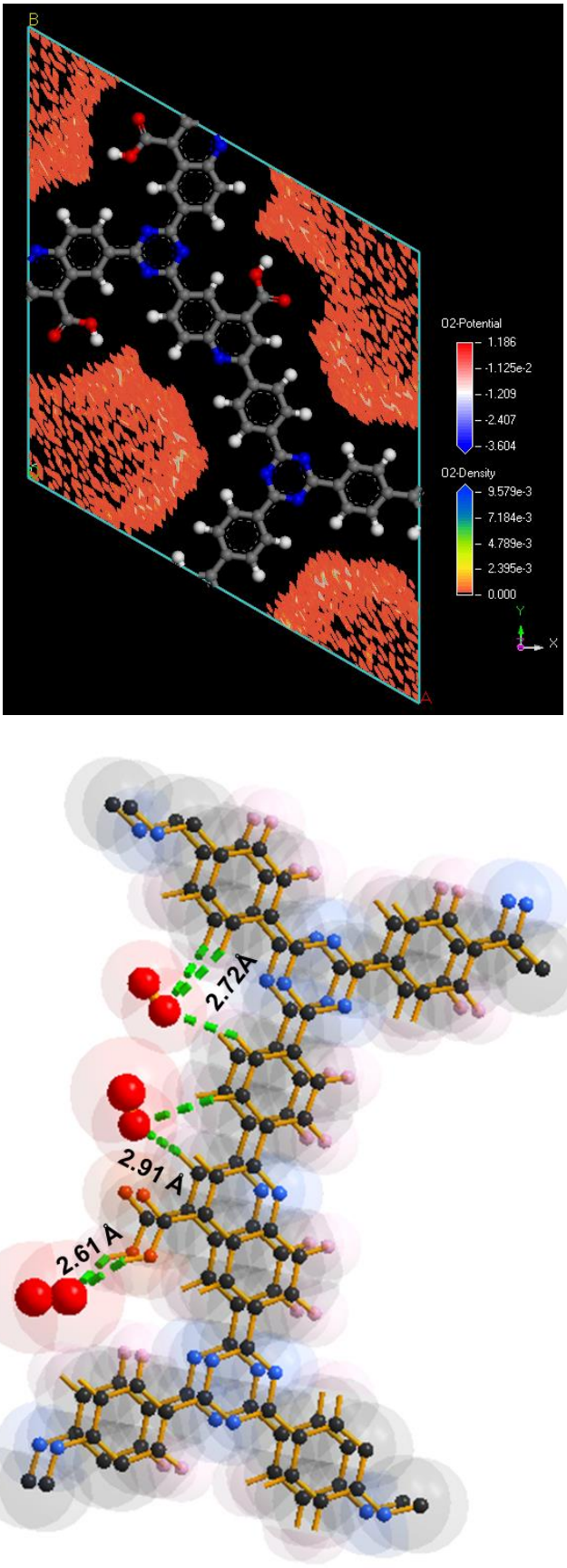

Figure S37. CBMC molecular simulation: adsorption position and probability distribution plot of O_2 at 1 bar in **DMCR-1**.

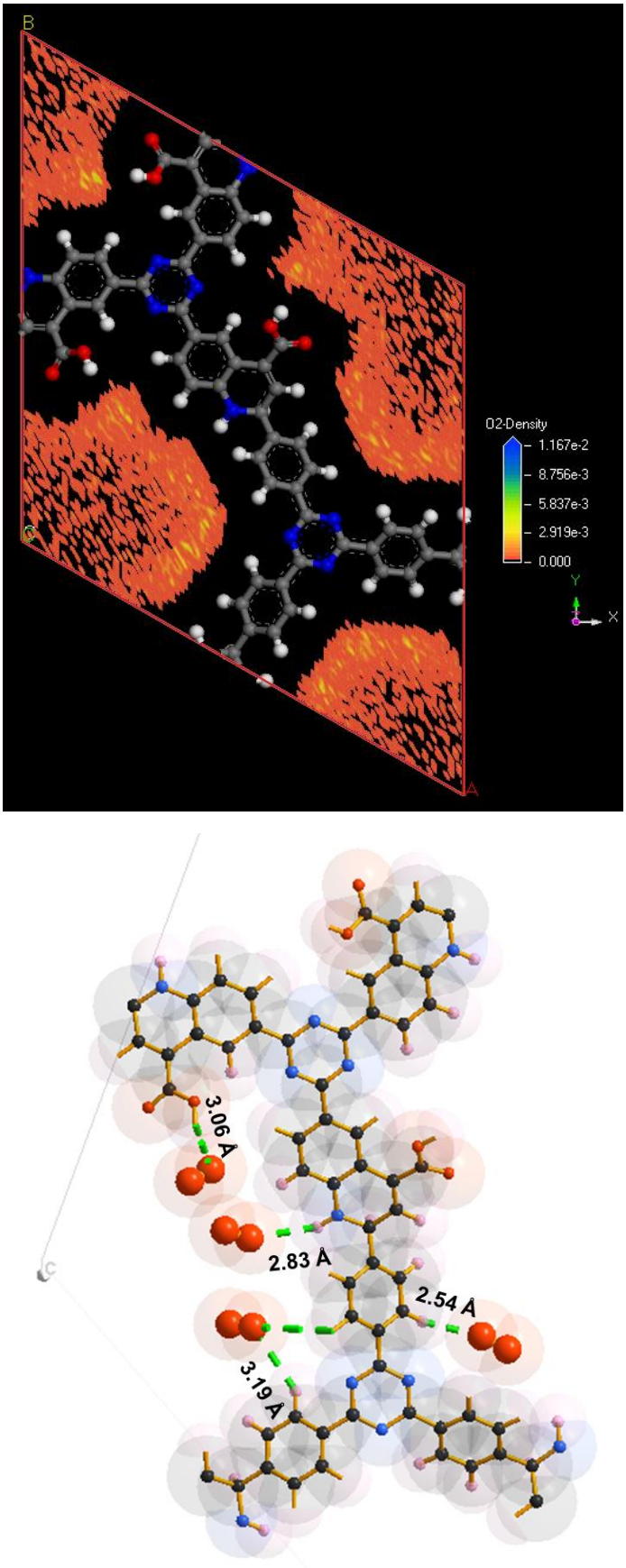

Figure S38. CBMC molecular simulation: adsorption position and probability distribution plot of O_2 at 1 bar in **DMCR-1NH**.

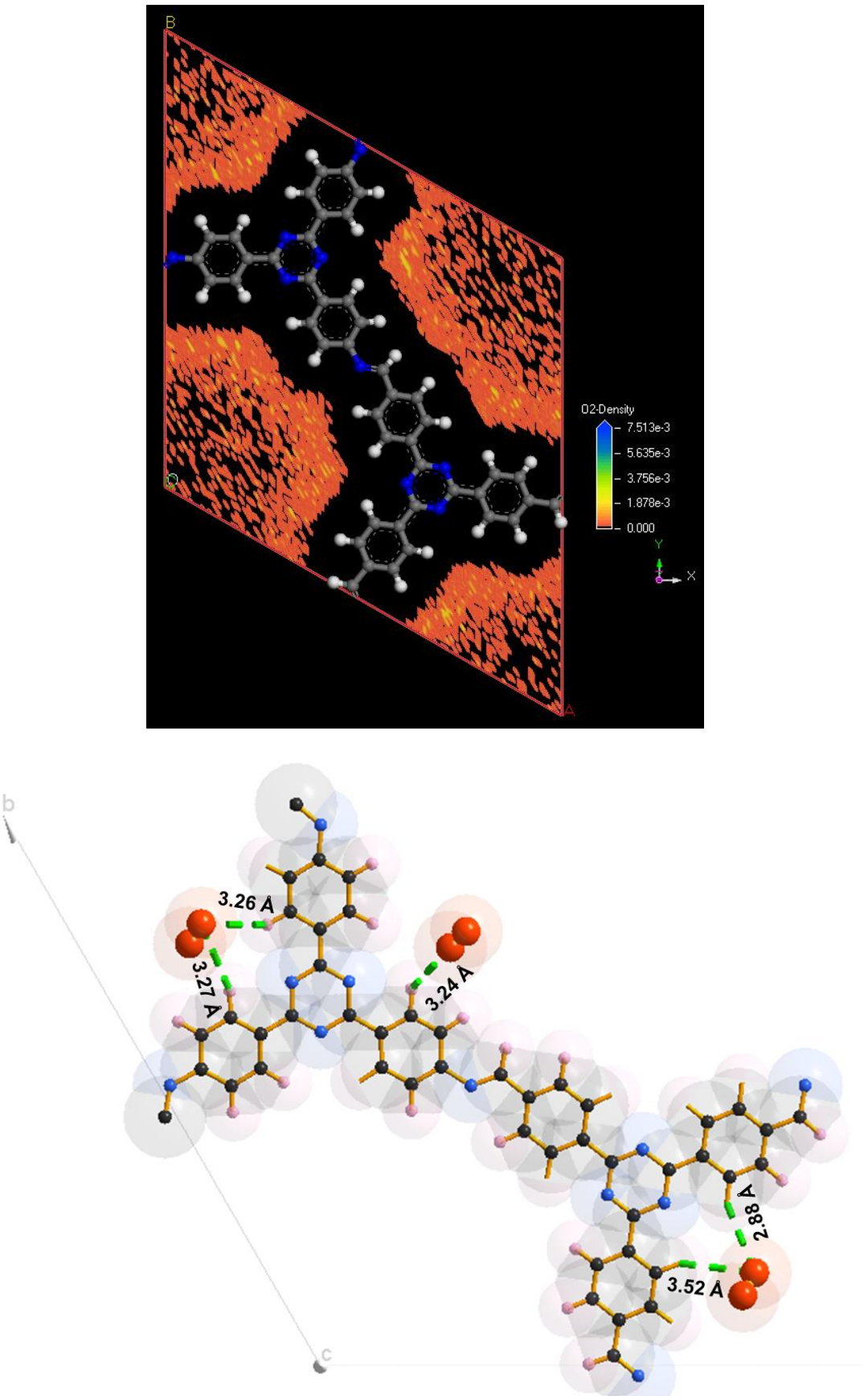

Figure S39. CBMC molecular simulation: adsorption position and probability distribution plot of O_2 at 1 bar in **Imine-1**.

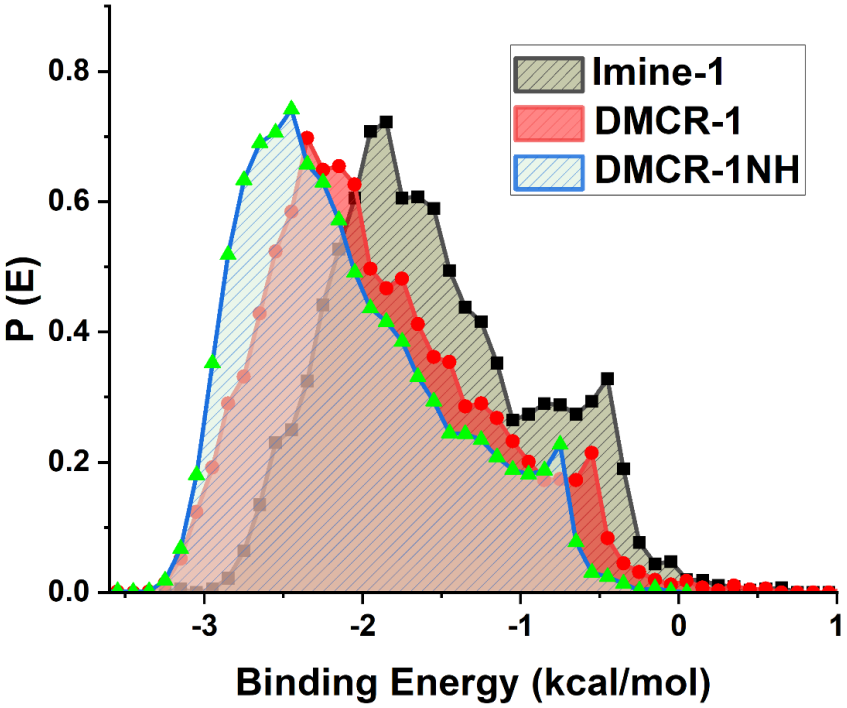

Figure S40. Binding energy of O_2 in presence of **DMCR-1**, **DMCR-1NH** and **Imine-1**.

Section 9. Photocatalytic Experiments

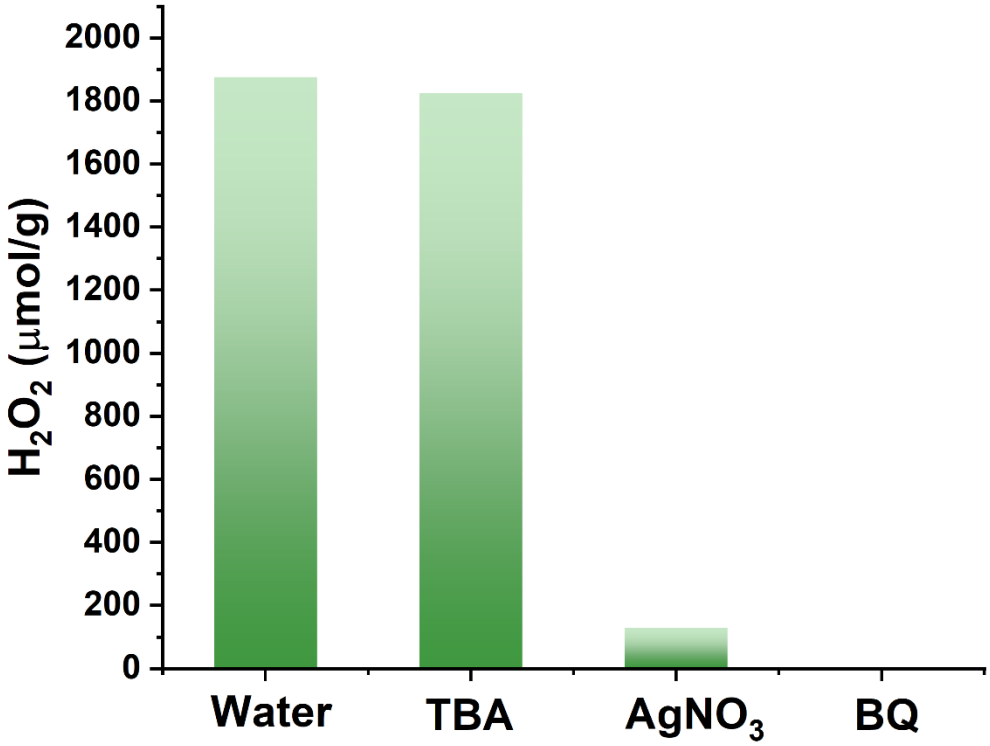

Figure S41. Photocatalytic H_2O_2 production for **DMCR-1** in neat water, with benzoquinone (BQ), *tert*-butyl alcohol (TBA) and $AgNO_3$ (5 mL 10 mM aqueous solution, 10 mg COF), all with 1 h illumination (Oriel Solar Simulator 300 W Xe lamp). $AgNO_3$, *tert*-butyl alcohol (TBA), and benzoquinone (BQ) act as electron (e^-), hydroxyl radical (·OH), and superoxide radical ($\cdot O_2^-$) scavengers.

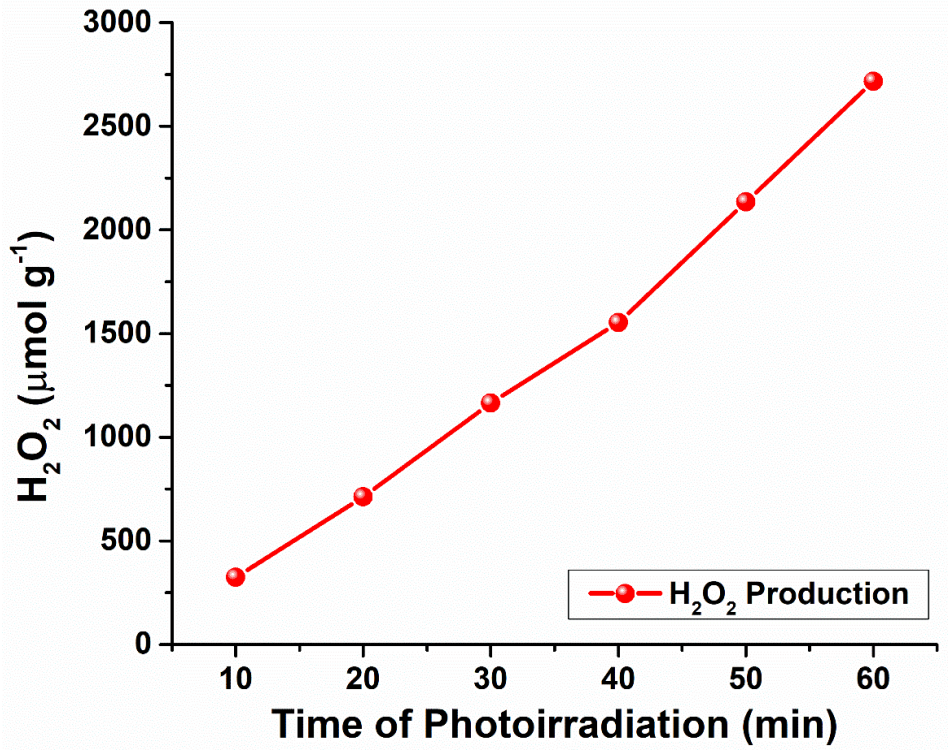

Figure S42. Time dependent H_2O_2 formation in water:IPA (10:1) for **DMCR-1NH** (5 mg of COF at 25 °C and λ = 420 nm).

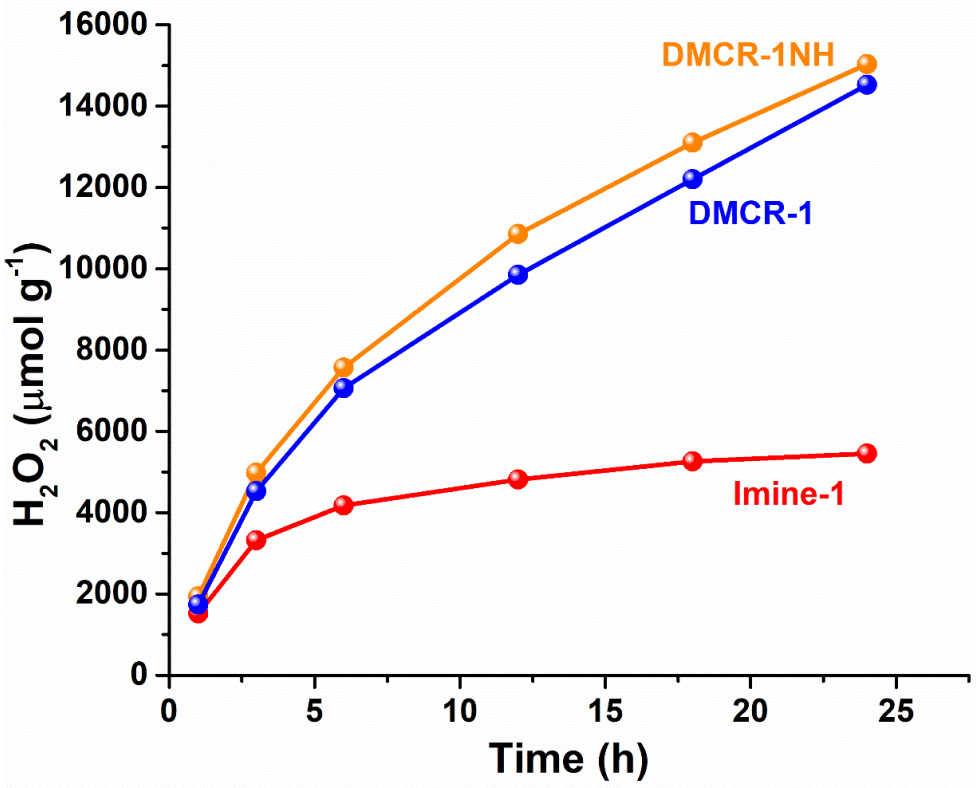

Figure S43. Time dependent long-term H_2O_2 formation in water:IPA (20:2) (10 mg of COFs at 25 °C and λ = 420 nm).

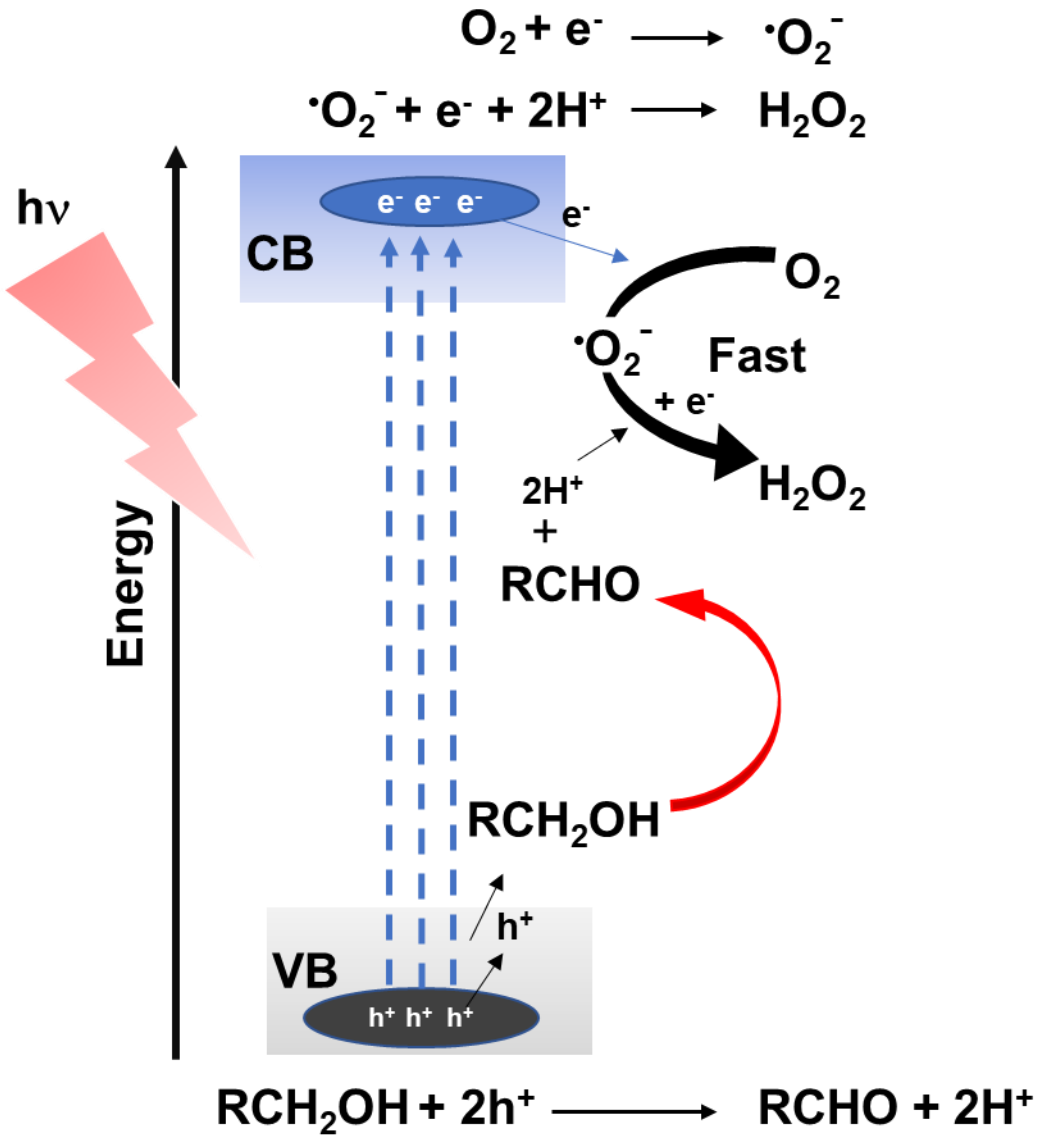

Figure S44. Proposed mechanism of H_2O_2 formation using COFs as photocatalyst.

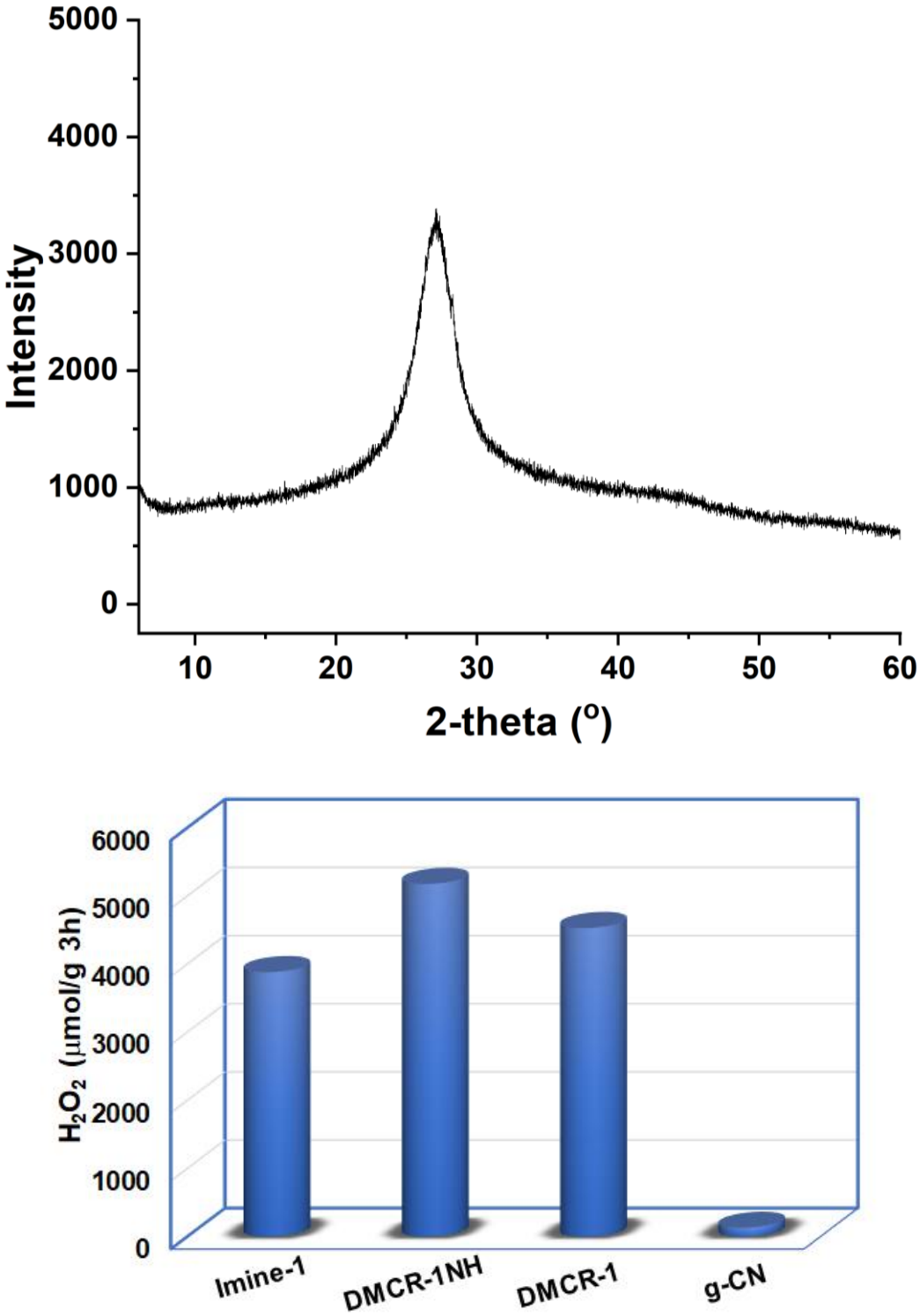

Figure S45. (Top) Experimental PXRD pattern of ***g*-CN**. (Bottom) Comparison of H_2O_2 production of *g*-CN with COFs.

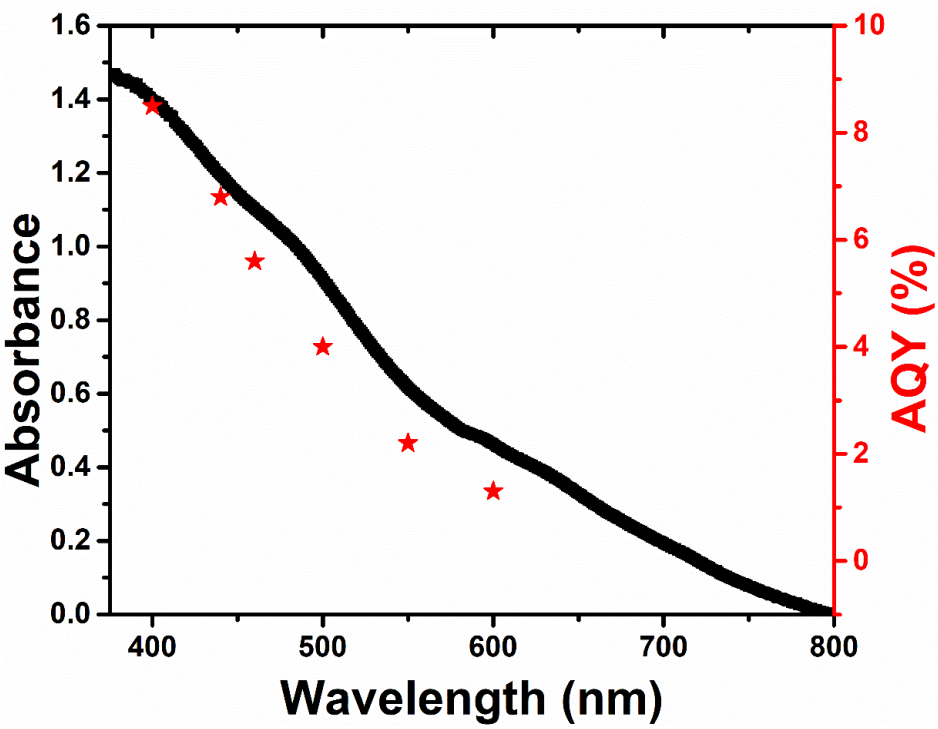

Figure S46. Wavelength dependent ACQ measurement for **DMCR-1**.

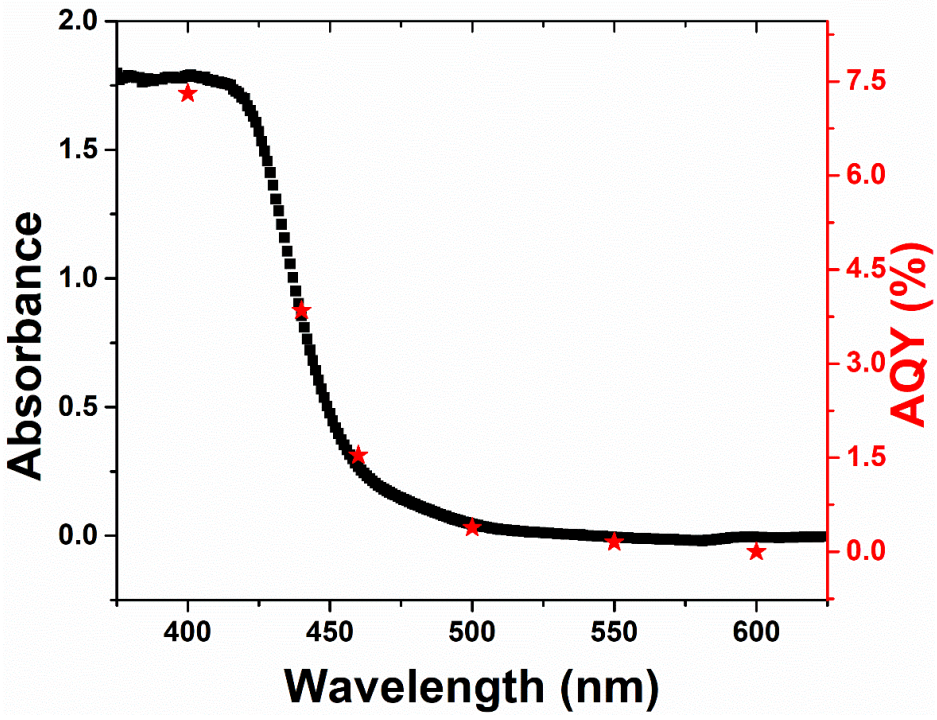

Figure S47. Wavelength dependent ACQ measurement for **Imine-1**.

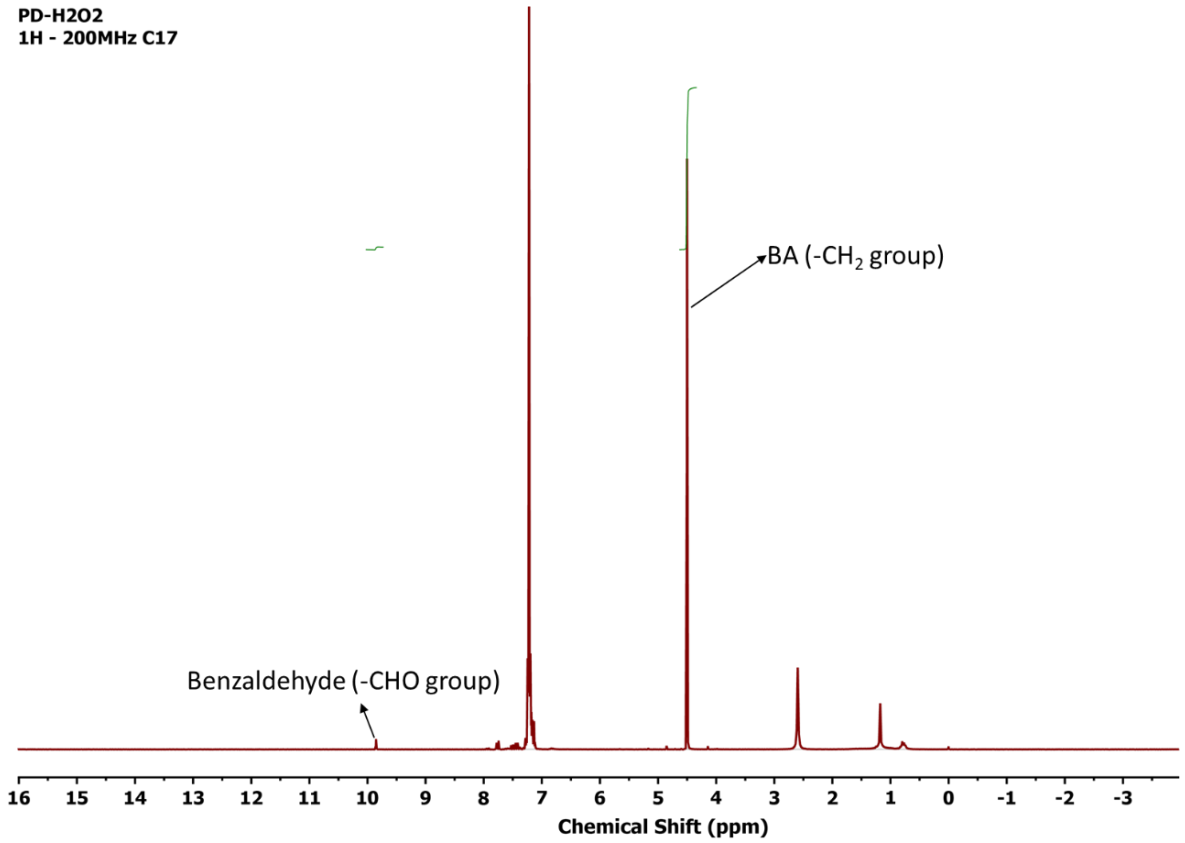

Figure S48. Formation of benzaldehyde after using BA as a sacrificial agent after long-term experiment in water/BA (10:1) system.

Recyclability Test

Each COF powder (10 mg) in 20:2 water:IPA (22 mL), was taken and then ultrasonicated for 10-15 min (to disperse the COF) after being capped under O_2 (10 min). After 2 h, 0.2 mL solution was solution was taken with a syringe equipped with a syringe filter. The amount of H_2O_2 produced was analysed with Peroxide test sticks. After every catalytic experiment, COFs were regenerated by simply washing with acetone and MeOH. Once regenerated by filtration and drying, the COF samples could be reused to produced H_2O_2 for at least five cycles.

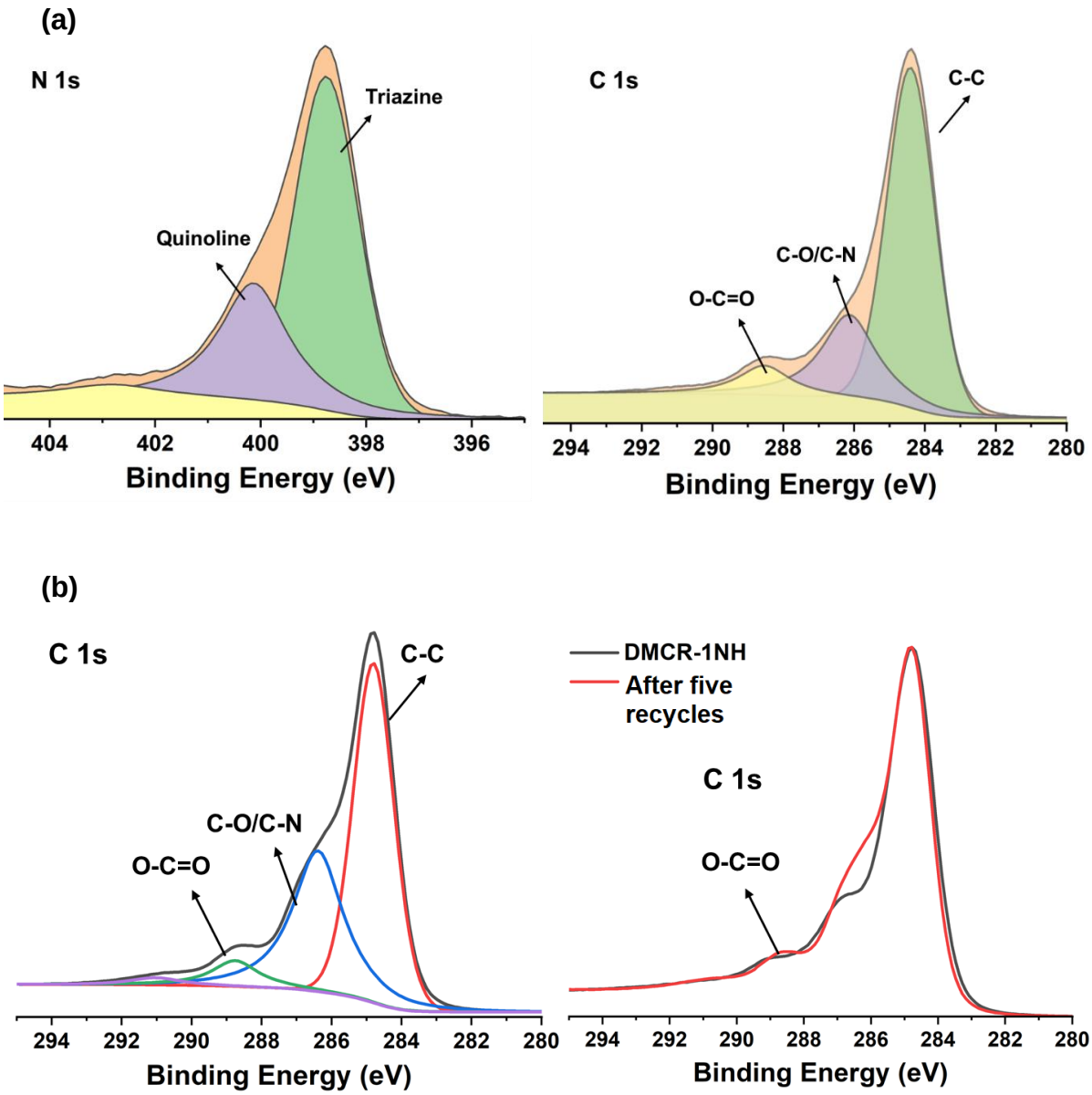

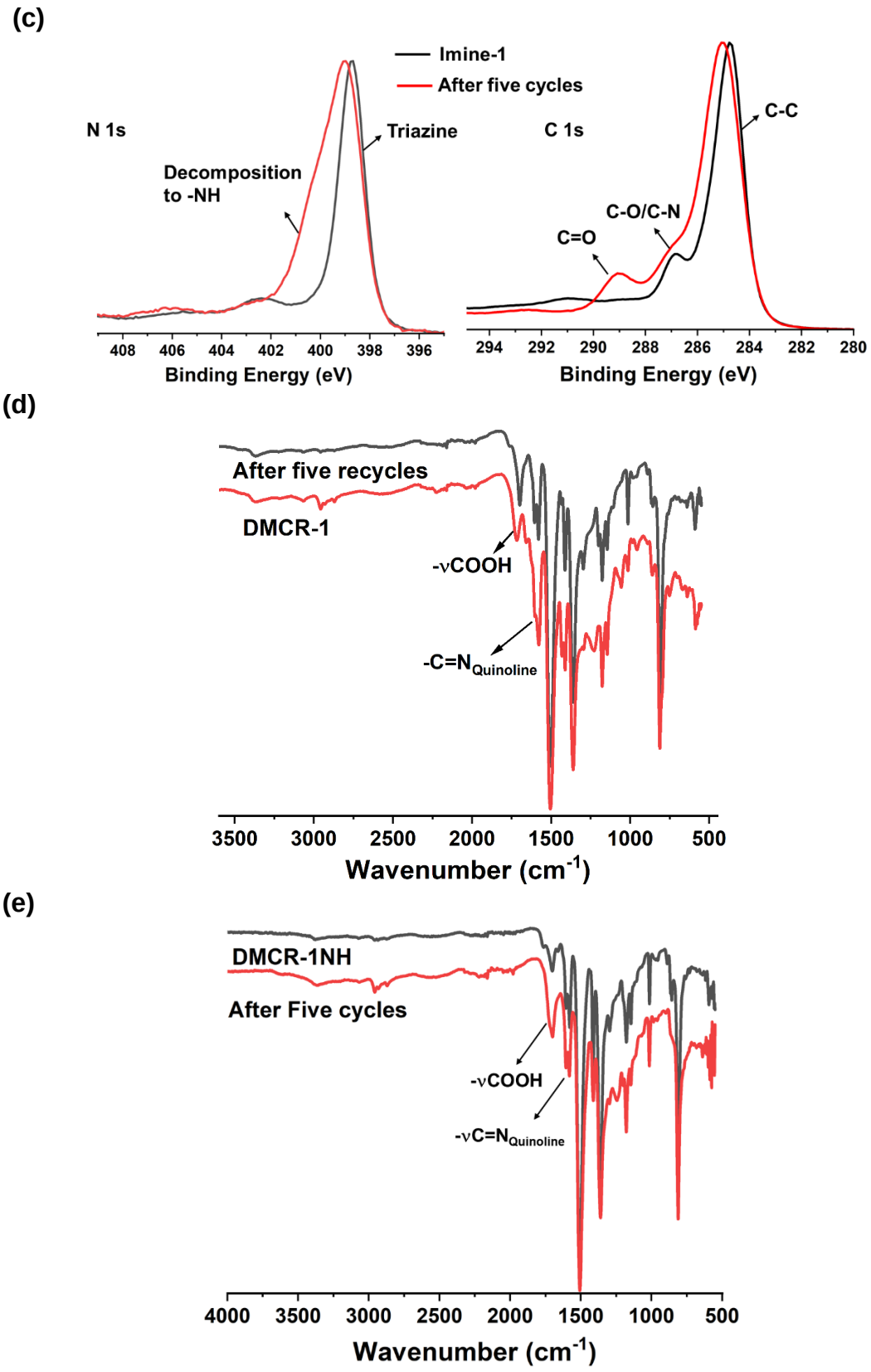

Figure S49. (a) N 1s and C 1s XPS of **DMCR-1**; (b) C 1s XPS of **DMCR-1NH;** (c) N 1s and C 1s XPS of **Imine-1** and FTIR spectra of (c) **DMCR-1** and (d) **DMCR-1NH** after 5 cycles.

Section 10. Synthesis and Characterization of DMCR-2 and DMCR-3

Synthesis of DMCR-2

A Pyrex glass tube (15 mL) was charged with 2,4,6-Tris(4-aminophenyl)triazine (Tta) (53.2 mg, 0.15 mmol), 1,3,5-Tris(4-formylphenyl)benzene (Tpa-CHO) (58.6 mg, 0.15 mmol), pyruvic acid (PA) (0.60 mmol, 60 μL), (DDQ) (10 mg, 0.04 mmol), 1.5 mL o-DCB and 1.5 mL *n*-BuOH. The tube was first sonicated for 30 minutes to form bulk solid and then flash frozen at 77 K (liquid N_2 bath) and degassed by three freeze-pump-thaw cycles. The internal pressure was evacuated to 10^{-3} mbar. The tube was sealed and heated at 120 °C for 3 days. The greenish brown precipitate was washed with acetone/MeOH several times and collected by filtration. Finally, the powder was dried in a normal oven at 80 °C. Yield = 89.7% (93 mg). Anal. Calcd (%): C, 76.5.; H, 3.38.; N, 9.39. Found (%): C, 76.21.; H, 3.18.; N, 9.90.

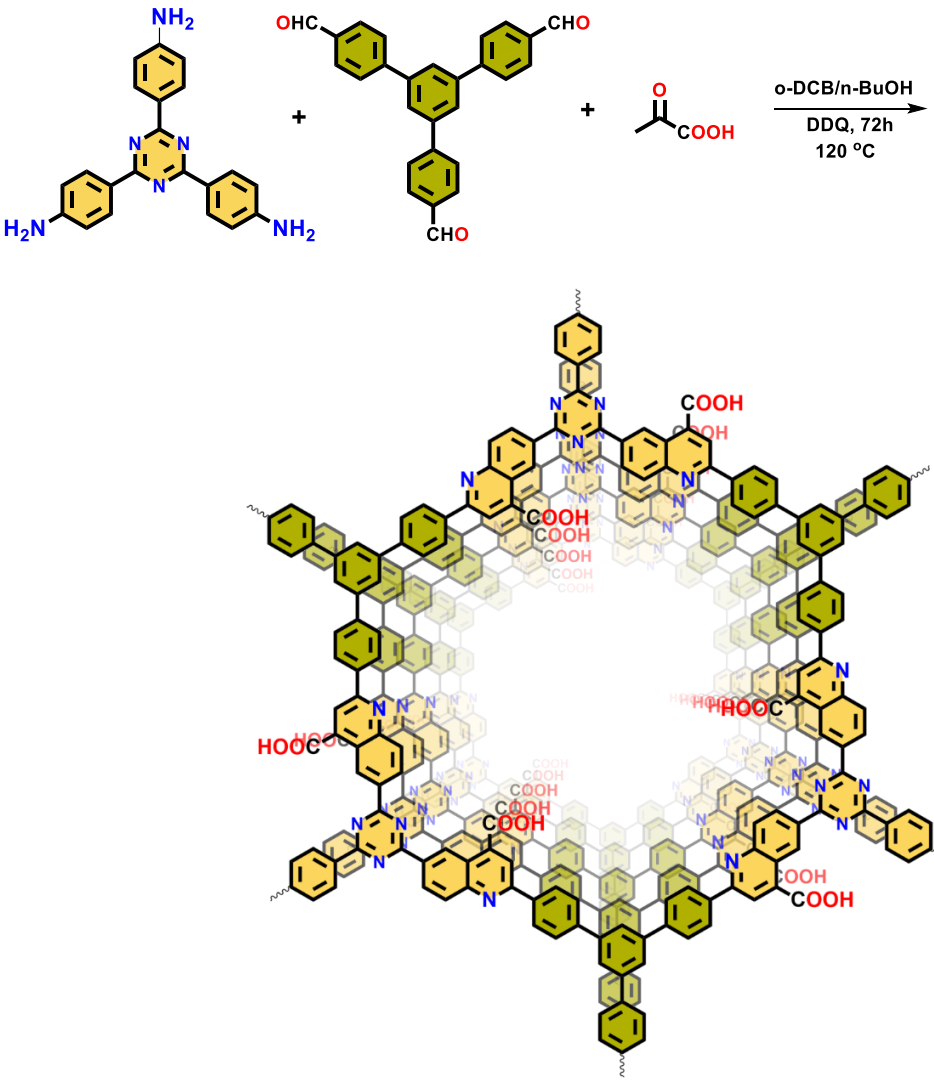

Scheme S5. Synthesis of **DMCR-2**.

Synthesis of DMCR-3

A Pyrex glass tube (15 mL) was charged with 2,4,6-Tris(4-aminophenyl)benzene (53.2 mg, 0.15 mmol), 1,3,5-Tris(4-formylphenyl)benzene (Tpa-CHO) (58.6 mg, 0.15 mmol), pyruvic acid (PA) (0.60 mmol, 60 μL), DDQ (10 mg, 0.04 mmol),1.5 mL *o*-DCB and 1.5 mL *n*-BuOH. The tube was first sonicated for 30 minutes to form bulk solid and then flash frozen at 77 K (liquid N_2 bath) and degassed by three freeze-pump-thaw cycles. The internal pressure was evacuated to 10^{-3} mbar. The tube was sealed and heated at 120 °C for 3 days. The brown precipitate was washed with acetone/MeOH several times and collected by filtration. Finally, the powder was dried in a normal oven at 80 °C. Yield = 82% (78 mg). Anal. Calcd. (%): C, 80.8.; H, 3.73.; N, 4.71. Found (%): C, 79.89.; H, 4.32.; N, 4.35.

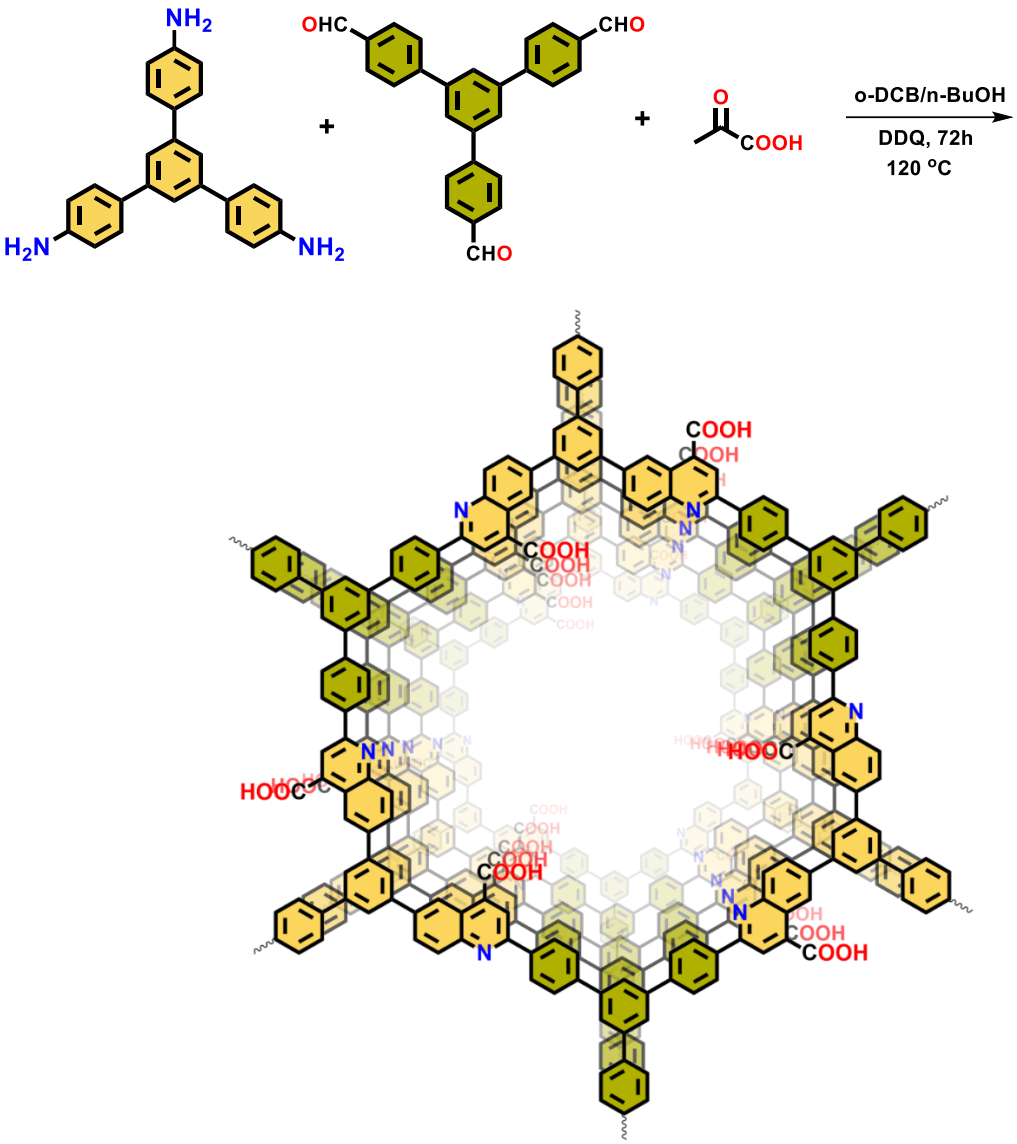

Scheme S6. Synthesis of **DMCR-3**.

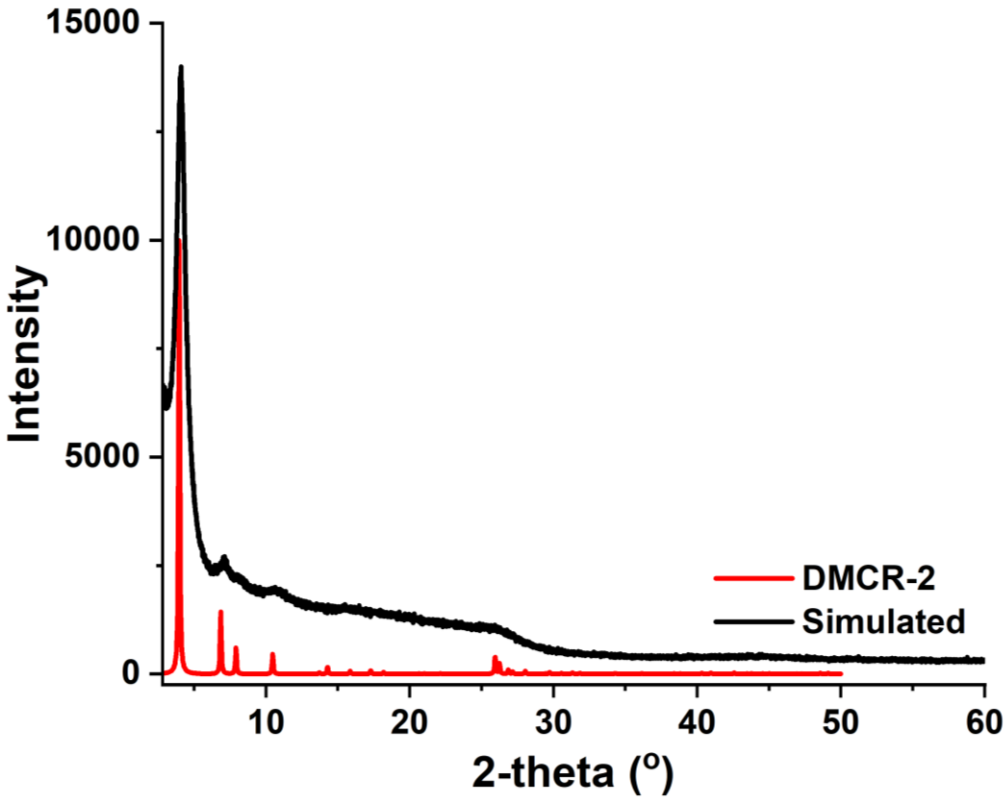

Figure S50. Simulated and experimental PXRD patterns of **DMCR-2**.

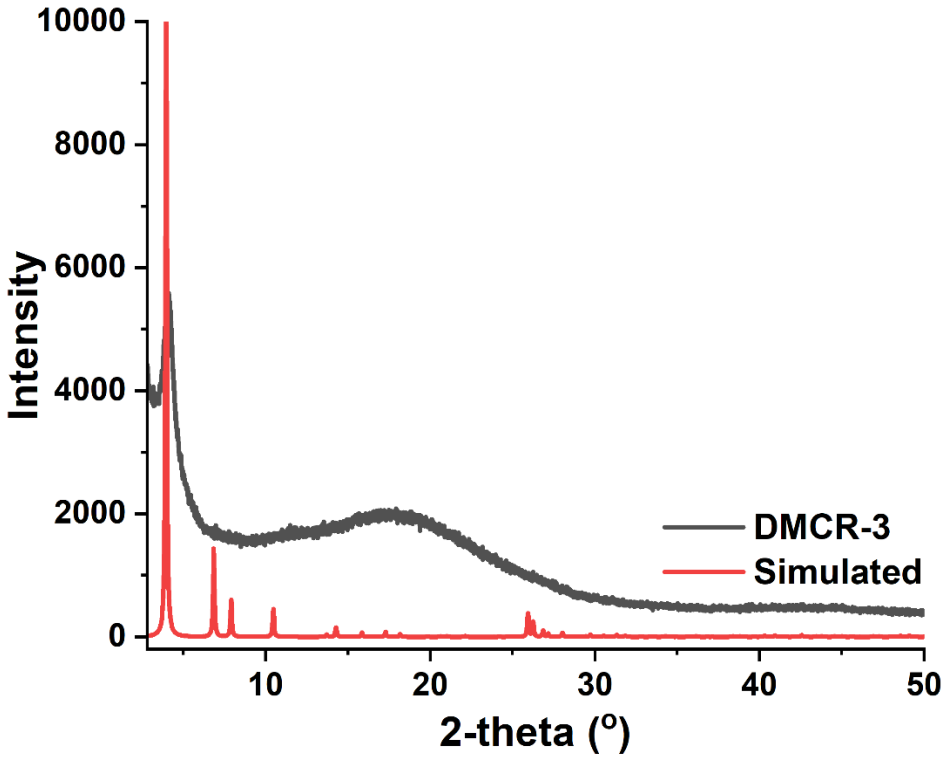

Figure S51. Simulated and experimental PXRD patterns of **DMCR-3**.

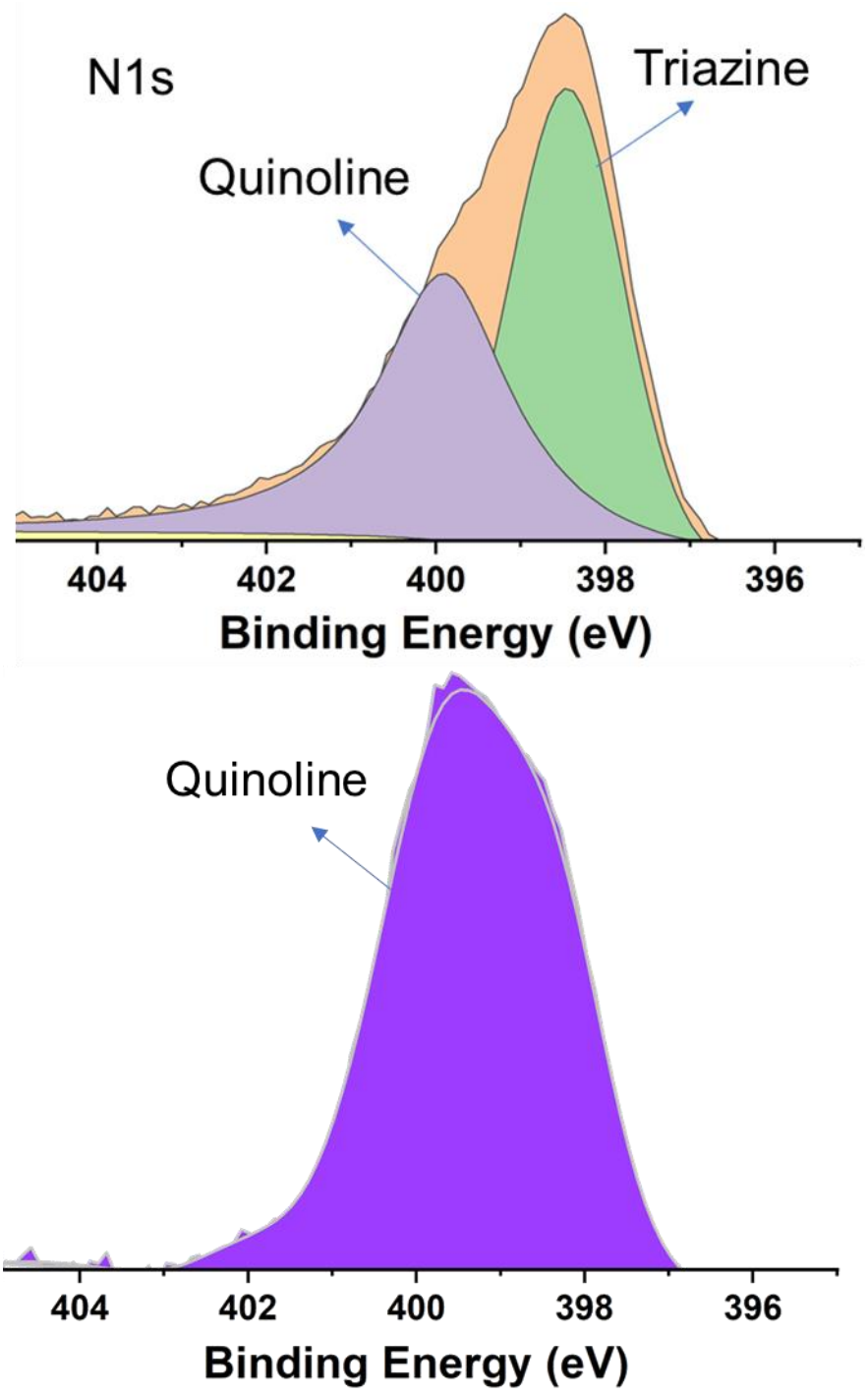

Figure S52. N(1s) XPS spectra of **DMCR-2** (Top) and **DMCR-3** (Bottom).

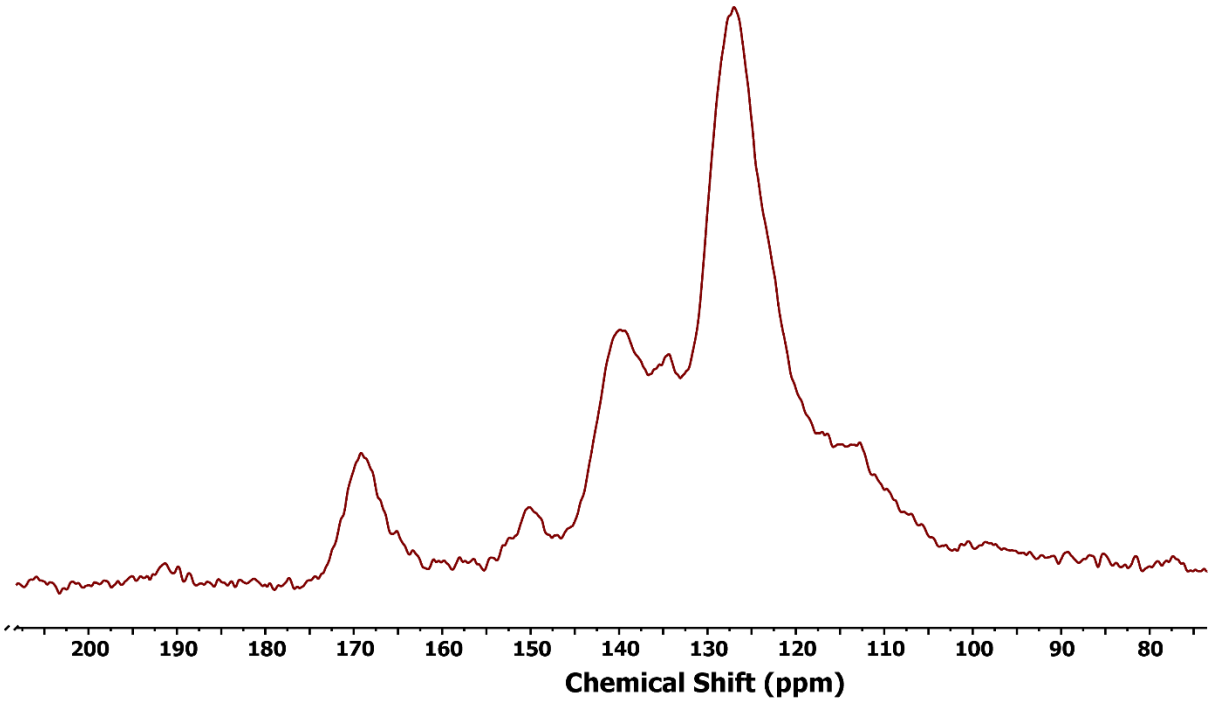

Figure S53. ^{13}C CP MAS NMR spectrum of **DMCR-2**.

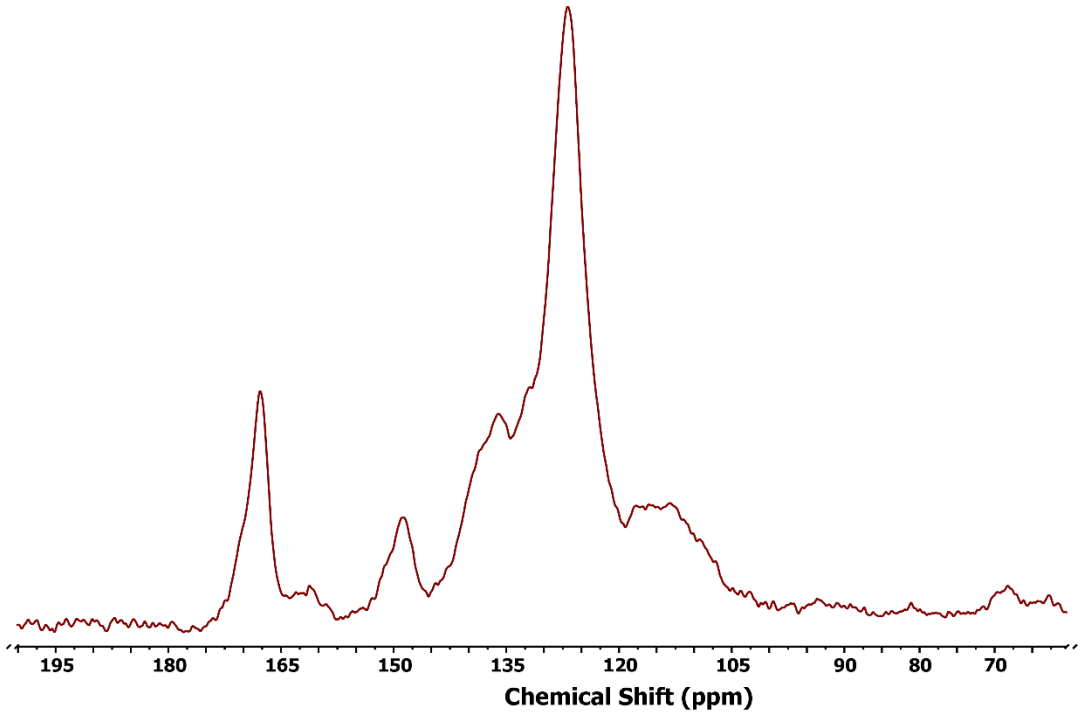

Figure S54. ^{13}C CP MAS NMR spectrum of **DMCR-3**.

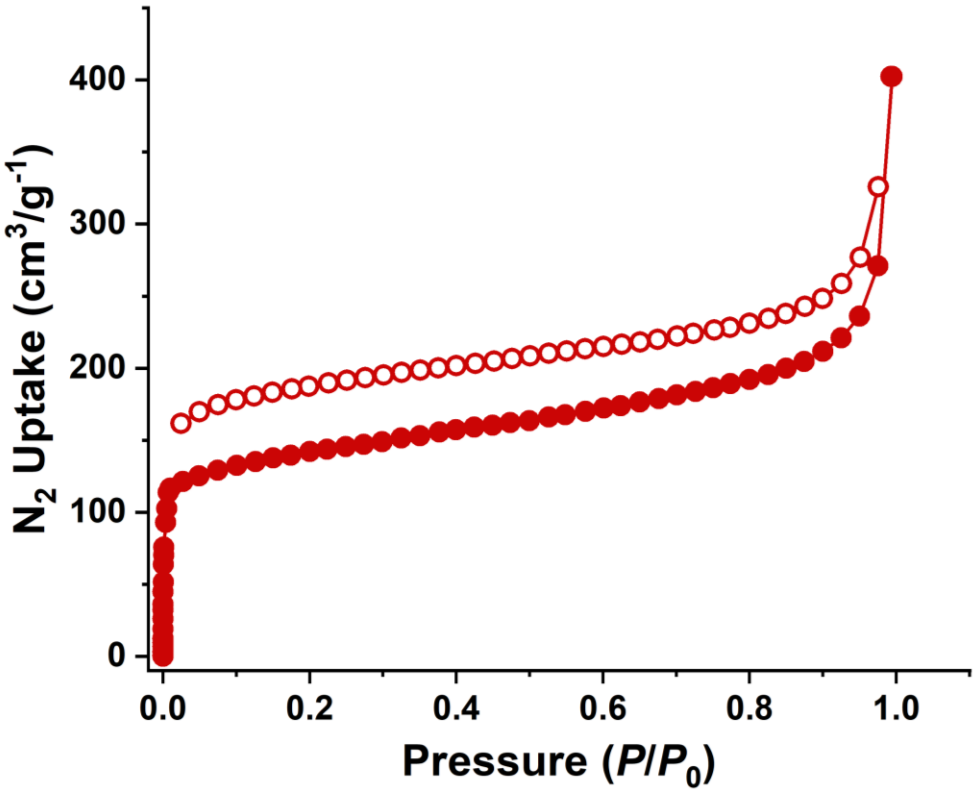

Figure S55. N_2 sorption isotherm of **DMCR-2** collected at 77 K with BET surface area 426 $m^2\,g^{-1}$.

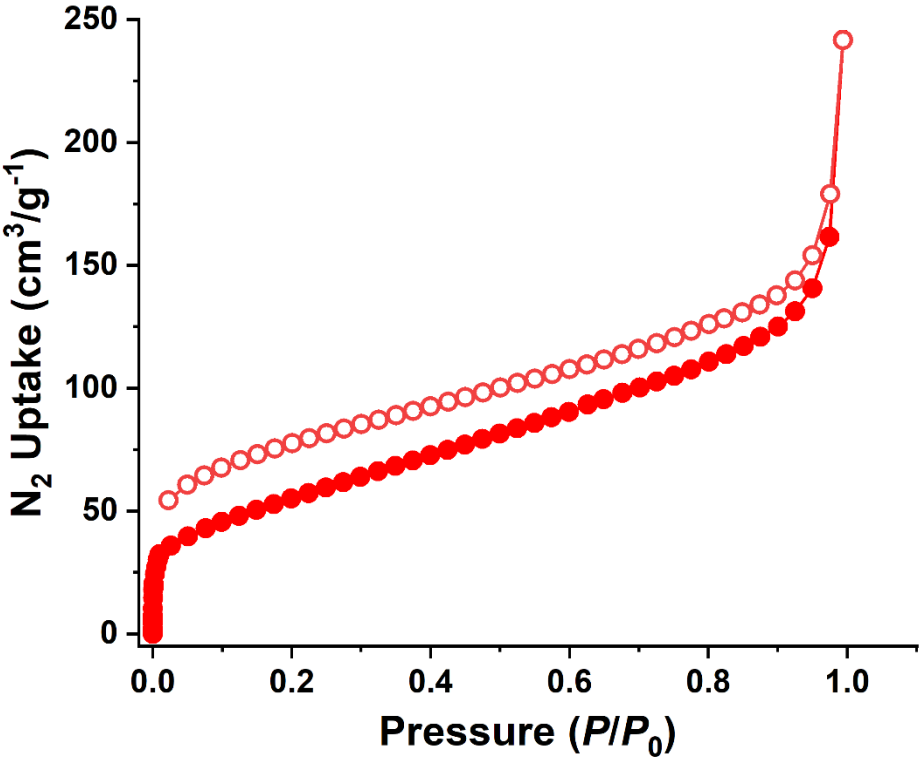

Figure S56. N_2 sorption isotherm of **DMCR-3** collected at 77 K with BET surface area 203 $m^2\,g^{-1}$.

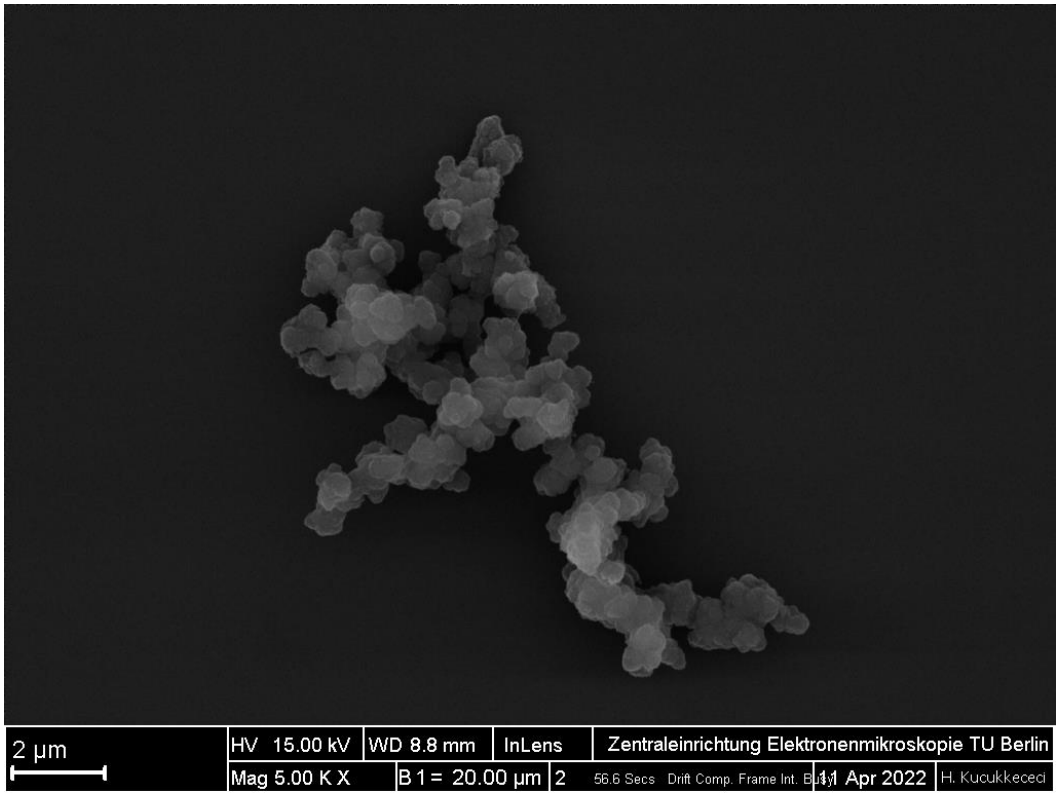

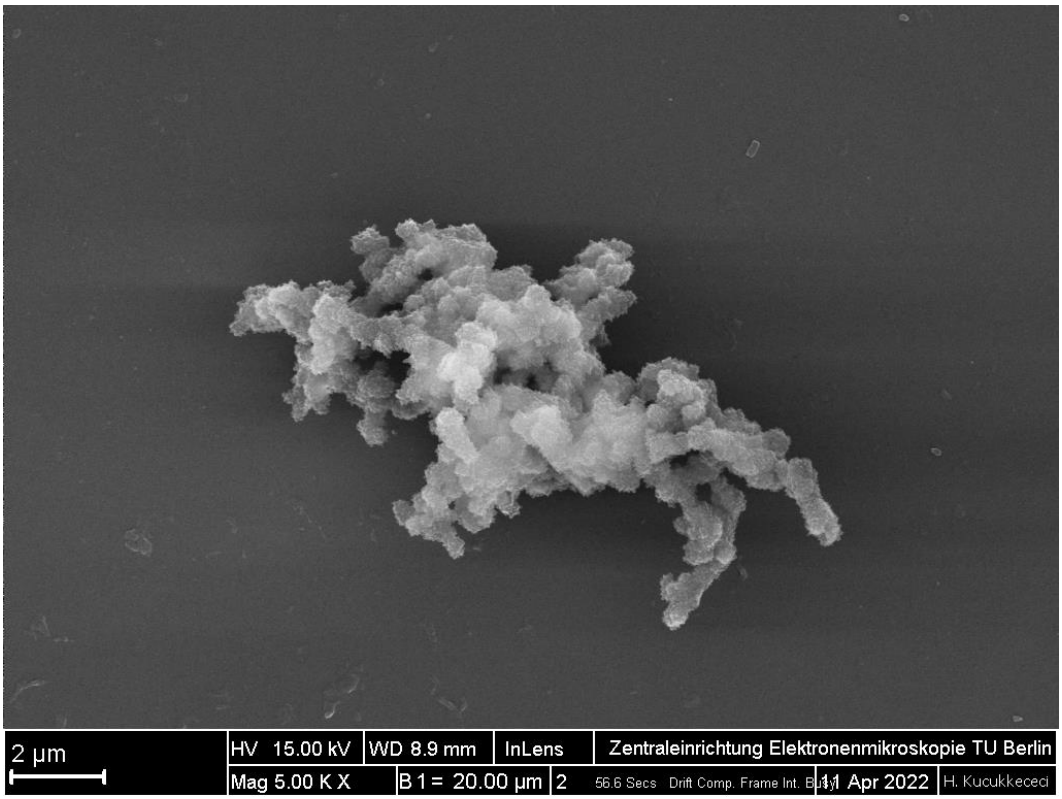

Figure S57. FESEM image of **DMCR-2** (top) and **DMCR-3** (bottom).

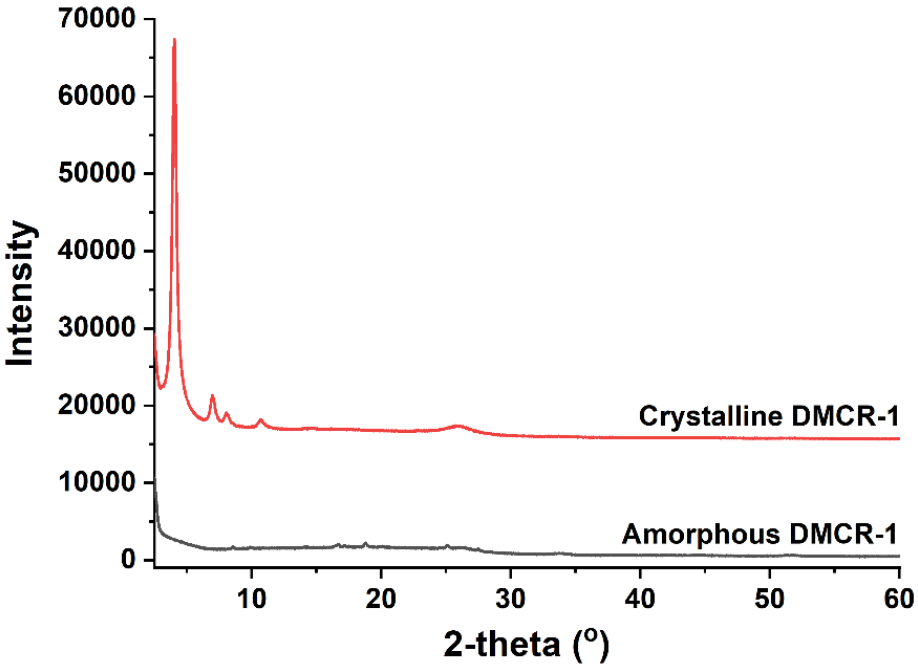

Figure S58. PXRD pattern of **amorphous DMCR-1** compared to PXRD pattern of **DMCR-1**.

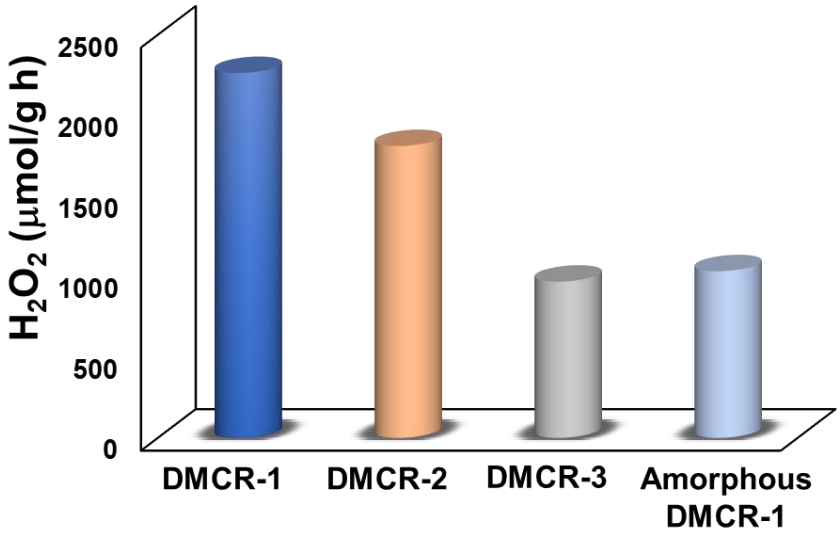

Figure S59. Comparison of H_2O_2 production after 1 h (5 mg of COFs in 10 mL water and 1 mL IPA, 1 h at 25 °C and λ = >420 nm).

Section 11: Comparison of H_2O_2 Production

Table S5. Comparison of H_2O_2 production for different materials.

Samples	H_2O_2 Production (μmol/h.g)	Irradiation Conditions	Solvent mixture	AQY (%)	Reference
DMCR-1	2264	λ = 420-700 nm	Water:IPA (10:1)	8.8	**This work**
DMCR-1NH	2588		Water:IPA (10:1)	10.2	
DMCR-2	1811		Water:IPA (10:1)		
DMCR-3	970		Water:IPA (10:1)		
Imine-1	1617		Water:IPA (10:1)	7.2	
DMCR-1NH	1941	Sunlight	Water:BA (10:1)		
DMCR-1NH	1319		Seawater:BA (10:1)		
SonoCOF-F2	197 (24 h)	λ = > 420 nm	Water	4.8	S4
EBA-COF	1820	λ = 420 nm	Water:EtOH (9:1)		S5
	1820		Water:IPA (9:1)		
	2550		Water:BA (9:1)		
BTEA-COF	780	λ = 420 nm	Water:EtOH (9:1)		
TAPD-$(Me)_2$ COF	97	λ = 420-700 nm	Water:EtOH (9:1)		S6
TAPD-$(OMe)_2$ COF	91	λ = 420-700 nm	Water:EtOH (9:1)		
DE7-M	266 (24h)	λ = > 420 nm	Water	8.7	S7
CTF-BDDBN	96.7	λ = 420-700 nm	Water		S8
CTF-EDDBN	56.7	λ = 420-700 nm	Water		
CTF-BPDCN	28.3	λ = 420-700 nm	Water		
OCN-500	106	λ = > 420 nm	Water	10.2	S9
COF-TfyBpy	1042	λ = 420-700 nm	Water		S10
g-C3N4	63	λ = > 420 nm	Water:EtOH (9:1)		S11
PEI/C3N4	4.2	λ = > 420 nm	Water	2.21	S12
PC-HM(g-C_3N_4)	268	λ = > 420 nm	Water:BA (1:1)		S13
Sb-SAPC15	470.5 (8h)	λ = > 420 nm	water	17.6	S14

CoPC-BTM-COF	2096	λ = > 400 nm	Water:EtOH (9:1)	7.2	S15
CoPC-DAB-COF	1815	λ = > 400 nm	Water:EtOH (9:1)	5.2	

References:

(S1) Zhang, Y.; Položij M.; Heine T. Statistical Representation of Stacking Disorder in Layered Covalent Organic Frameworks, *Chem. Mater.* **2022**, *34*, 2376-2381.
(S2) Rouquerol, J.; Rouquerol, F.; Llewellyn, P.; Maurin, G.; Sing, K. S. W.; *Adsorption by Powders and Porous Solids (Second Edition)*. Academic Press, Oxford: 2014.

(S3) Osterrieth, J. W. M.; Rampersad J.; Madden, D.; Rampal, N.; Skoric, L.; Connolly B.; Allendorf, M. D.; Stavila, V.; Snider, J. L.; Ameloot, R.; Marreiros, J.; Ania, C.; Azevedo, D.; Vilarrasa-Garcia, E.; Santos, B. F.; Bu X.-H.; Chang, Z.; Bunzen H.; Champness, N. R.; Griffin, S. L.; Chen, B.; Lin, R.-B.; Coasne, B.; Cohen, S.; Moreton, J. C.; Colón, Y. J.; Chen, L.; Clowes, R.; Coudert, F.-X.; Cui Y.; Hou, B.; D'Alessandro, D. M.; Doheny, P. W.; Dincă, M.; Sun C.; Doonan, C.; Huxley, M. T.; Evans, J. D.; Falcaro P.; Ricco R.; Farh,a O.; Idrees, K. B.; Islamoglu, T.; Feng P.; Yang, H.; Forgan, R. S.; Bara, D.; Furukawa, S.; Sanchez, E.; Gascon, J.; Telalović S.; Ghosh, S. K.; Mukherjee, S.; Hill, M. R.; Sadiq, M. M.; Horcajada, P.; Salcedo-Abraira, P.; Kaneko, K.; Kukobat R.; Kenvin, J.; Keskin, S.; Kitagawa, S.; Otake K.-i.; Lively, R. P.; DeWitt, S. J. A.; Llewellyn, P.; Lotsch, B. V.; Emmerling, S. T.; Pütz A. M.; Martí-Gastaldo C.; Padial, N. M.; García-Martínez J.; Linares, N.; Maspoch, D.; Suárez del Pino, J. A.; Moghadam, P.; Oktavian, R.; Morris, R. E.; Wheatley, P. S.; Navarro, J.; Petit, C.; Danaci, D.; Rosseinsky, M. J.; Katsoulidis, A. P.; Schröder, M.; Han, X.; Yang, S.; Serre, C.; Mouchaham, G.; Sholl, D. S.; Thyagarajan, R.; Siderius, D.; Snurr, R. Q.; Goncalves, R. B.; Telfer, S.; Lee, S. J.; Ting, V. P.; Rowlandson, J. L.; Uemura, T.; Iiyuka, T. How Reproducible are Surface Areas Calculated from the BET Equation? *Adv. Mater.* **2022**, *34*, 2201502.

(S4) Zhao, W.; Yan, P.; Li, B.; Bahri, M.; Liu, L.; Zhou, X.; Clowes, R.; Browning, N. D.; Wu, Y.; Ward, J. W.; Cooper, A. I. Accelerated Synthesis and Discovery of Covalent Organic Framework Photocatalysts for Hydrogen Peroxide Production. *J. Am. Chem. Soc.* **2022**, *144*, 9902–9909.

(S5) Zhai, L.; Xie, Z.; Cui, C.-X.; Yang, X.; Xu, Q.; Ke, X.; Liu, M.; Qu, L.-B.; Chen, X.; Mi, L. Constructing Synergistic Triazine and Acetylene Cores in Fully Conjugated Covalent Organic Frameworks for Cascade Photocatalytic H_2O_2 Production. *Chem. Mater.* **2022**, *34*, 5232–5240.

(S6) Krishnaraj, C.; Jena, H. S.; Bourda, L.; Laemont, A.; Pachfule, P.; Roeser, J.; Chandran, C. V.; Borgmans, S.; Rogge, S. M. J.; Leus, K.; Stevens, C. V.; Martens, J. A.; Speybroeck, V. V.; Breynaert, E.; Thomas, A.; Voort, P. V. D. Strongly Reducing

(Diarylamino)benzene-Based Covalent Organic Framework for Metal-Free Visible Light Photocatalytic H_2O_2 Generation. *J. Am. Chem. Soc.* **2020**, *142*, 20107−20116.

(S7) Liu, L.; Gao, M.; Yang, H.; Wang, X.; Li, X.; Cooper, A. I. Linear Conjugated Polymers for Solar-Driven Hydrogen Peroxide Production: The Importance of Catalyst Stability. *J. Am. Chem. Soc.* **2021**, *143*, 19287-19293.

(S8) Chen, L.; Wang, L.; Wan, Y.; Zhang, Y.; Qi, Z.; Wu, X.; Xu, H. Acetylene and Diacetylene Functionalized Covalent Triazine Frameworks as Metal-Free Photocatalysts for Hydrogen Peroxide Production: A New Two-Electron Water Oxidation Pathway. *Adv. Mater.* **2020**, *32*, 1904433.

(S9) Wei, Z.; Liu, M.; Zhang, Z.; Yao, W.; Tan, H.; Zhu, Y. Efficient Visible-Light-Driven Selective Oxygen Reduction to Hydrogen Peroxide by Oxygen-Enriched Graphitic Carbon Nitride Polymers. *Energy Environ. Sci.* **2018**, *11*, 2581-2589.

(S10) Kou, M.; Wang, Y.; Xu, Y.; Ye, L.; Huang, Y.; Jia, B.; Li, H.; Ren, J.; Deng, Y.; Chen, J.; Zhou, Y.; Lei, K.; Wang, L.; Liu, W.; Huang, H.; Ma, T. Molecularly Engineered Covalent Organic Frameworks for Hydrogen Peroxide Photosynthesis. *Angew Chem., Int. Ed.* **2022**, *61*, e202200413.

(S11) Shiraishi, Y.; Kanazawa, S.; Sugano, Y.; Tsukamoto, D.; Sakamoto, H.; Ichikawa, S.; Hirai, T. Highly Selective Production of Hydrogen Peroxide on Graphitic Carbon Nitride (g-C3N4) Photocatalyst Activated by Visible Light. *ACS Catal.* **2014**, *4*, 774-780.

(S12) Zeng, X.; Liu, Y.; Kang, Y.; Li, Q.; Xia, Y.; Zhu, Y.; Hou, H.; Uddin, M. H.; Gengenbach, T. R.; Xia, D.et al. Simultaneously Tuning Charge Separation and Oxygen Reduction Pathway on Graphitic Carbon Nitride by Polyethylenimine for Boosted Photocatalytic Hydrogen Peroxide Production. *ACS Catal.* **2020**, *10*, 3697-3706.

(S13) Ou, H.; Tang, C.; Chen, X.; Zhou, M.; Wang, X. Solvated Electrons for Photochemistry Syntheses Using Conjugated Carbon Nitride Polymers. *ACS Catal*. **2019**, *9*, 2949-2955.

(S14) Teng, Z.; Zhang, Q.; Yang, H.; Kato, K.; Yang, W.; Lu, Y.; Liu, S.; Wang, C.; Yamakata, A.; Su, C.et al. Atomically Dispersed Antimony on Carbon Nitride for the Artificial Photosynthesis of Hydrogen Peroxide. *Nat. Catal.* **2021**, *4*, 374-384.

(S15) Zhi, Q.; Liu, W.; Jiang, R.; Zhan, X.; Jin, Y.; Chen, X.; Yang, X.; Wang, K.; Cao, W.; Qi, D.; Jiang, J. Piperazine-Linked Metalphthalocyanine Frameworks for Highly Efficient Visible-Light-Driven H_2O_2 Photosynthesis. *J. Am. Chem. Soc.* **2022**, *144*, 21328-21336.